

Nanoscale

Accepted Manuscript



This is an *Accepted Manuscript*, which has been through the Royal Society of Chemistry peer review process and has been accepted for publication.

Accepted Manuscripts are published online shortly after acceptance, before technical editing, formatting and proof reading. Using this free service, authors can make their results available to the community, in citable form, before we publish the edited article. We will replace this *Accepted Manuscript* with the edited and formatted *Advance Article* as soon as it is available.

You can find more information about *Accepted Manuscripts* in the [Information for Authors](#).

Please note that technical editing may introduce minor changes to the text and/or graphics, which may alter content. The journal's standard [Terms & Conditions](#) and the [Ethical guidelines](#) still apply. In no event shall the Royal Society of Chemistry be held responsible for any errors or omissions in this *Accepted Manuscript* or any consequences arising from the use of any information it contains.

FEATURE ARTICLE

Bismuth Oxyhalide Nanomaterials: Layered Structures Meet Photocatalysis

Cite this: DOI: 10.1039/x0xx00000x

Jie Li,^{a,b} Ying Yu,^{a,b} and Lizhi Zhang^{*a}

Received 00th January 2012,
Accepted 00th January 2012

DOI: 10.1039/x0xx00000x

www.rsc.org/

In recent years layered bismuth oxyhalide nanomaterials have received more and more concerns as promising photocatalysts because their unique layered structures endow them with fascinating physicochemical properties and thus great potential photocatalytic applications for environment remediation and energy harvesting. In this article we explore the synthesis strategies and growth mechanisms of layered bismuth oxyhalide nanomaterials, and then propose design principles of tailoring layered configuration to control nanoarchitectures for high efficient photocatalysis. Subsequently, we focus on their layered structure dependent properties including pH related crystal facet exposure and phase transformation, and facet-dependent photoactivity and molecular oxygen activation pathways, so as to clarify the origin of layered structure dependent photoreactivity. Furthermore, we summarize various strategies of modulating the composition and arrangement of layered structures to enhance the photoactivity of nanostructured bismuth oxyhalides via internal electric field tuning, dehalogenation effect, surface functionalization, doping, plasmon modification, and heterojunction construction, which may offer efficient guidance for the design and construction of high-performance bismuth oxyhalide-based photocatalysis systems. Finally, we highlight some crucial issues in engineering the layered-structure mediated properties of bismuth oxyhalide photocatalysts and give tentative suggestions for future research on increasing their photocatalytic performance.

1. Introduction

Recent years have seen worldwide research interests on layered materials such as atomically-thick graphene, hexagonal boron nitride, transition metal dichalcogenides, perovskites, layered double hydroxides, graphitic carbon nitrides, because they are fundamentally and technologically intriguing for a variety of potential applications in electronics, catalysis, and energy storage.¹⁻¹⁶ Of these layered materials, bismuth oxyhalides BiOX (X = Cl, Br, and I) belong to a new class of promising layered materials for photocatalytic energy conversion and environment remediation because of their unique layered-structure mediated fascinating physicochemical properties and suitable band-structure, as well as high chemical and optical stability, nontoxicity, low cost, and corrosion resistance.¹⁷⁻¹⁹ As a group of V-VI-VII ternary compound semiconductors, bismuth oxyhalides with a tetragonal matlockite (PbFCl-type) structure (space group P4/nmm) crystallize into layered structures consisting of [X-Bi-O-Bi-X] slices stacked

together by the nonbonding (van der Waals) interaction through the halogen atoms along the c-axis.²⁰ In each [X-Bi-O-Bi-X] layer, a bismuth center is surrounded by four oxygen and four halogen atoms, which thus generate an asymmetric decahedral geometry. The strong intralayer covalent bonding and the weak interlayer van der Waals interaction give rise to highly anisotropic structural, electrical, optical, and mechanical properties, which endow BiOX with promising application potential on photocatalytic wastewater and indoor-gas purification, water splitting, organic synthesis, and selective oxidation of alcohol.²¹⁻³¹

It was generally accepted that controlling the size of materials at the nanometer scale could induce the emergence of new physical and chemical properties.³²⁻³⁴ As the size of the materials decreased, the percentage of the surface atoms with more dangling bonds and the surface-to-volume ratio increased dramatically. This would result in enhanced chemical activity, lowered melting point, increased phase transition pressure, and higher solubility in comparison with

their bulk counterparts. Therefore, it is of great importance to synthesize nanostructured bismuth oxyhalide materials with enhanced photocatalytic activity.

To date, many bismuth oxyhalide nanostructures ranging from nanosheets, nanobelts, nanofibers, nanowires, nanoflowers and hollow nanostructure, etc. have been successfully fabricated via a variety of synthetic routes.³⁵⁻⁶⁸ These routes can be briefly categorized into six kinds, which generally include hydrothermal and solvothermal syntheses, templated synthesis, sonochemical synthesis, interface-mediated synthesis, reversed-phase microemulsion synthesis, and anion exchange synthesis, etc. The advances in each synthetic method have inspired multiple motivations to drive the rapid development of bismuth oxyhalide nanomaterials in the photocatalysis field. Although intensive efforts were devoted to the design of well-defined nanostructures to optimize the photoreactivity of bismuth oxyhalides, much less attention was paid to the intrinsic roles of unique layered structure in improving the photocatalytic activity and the fine manipulation of layered structure. The unique layered structure endowed bismuth oxyhalide nanomaterials with two main fascinating advantages. First, the layered structure of bismuth oxyhalide is sensitive to the pH value of surrounding environment. Reasonably tuning the pH value of growth environment of bismuth oxyhalide nanocrystals resulted in the transformation of crystal phase to generate new layered semiconductors of suitable band structure favorable for the improvement of light absorbance capacity, charge carrier transfer, and the redox potential, and also enabled the facet-selective growth of layered structure to realize desirable facet exposure.^{69,70} Through crystal facet engineering of bismuth oxyhalide nanomaterials, the interaction of molecular oxygen and photogenerated electrons could be finely tuned, which allowed us to selectively manipulate the molecular oxygen activation process and the photocatalytic reactions.⁷¹ Second, the non-uniform charge distribution between [Bi₂O₂] and halogen slices in the nanosheets would polarize the related atoms and orbitals to form internal electric fields along the crystal orientation perpendicular to the [X] and [Bi₂O₂] layers.^{20,69,72} It is well established that the photocatalytic process with semiconductor material involves light photoexcitation, the subsequent separation and transfer of photogenerated charge carriers, and the final redox reactions between the charge carriers and the substances on the semiconductor surface, thus the charge dynamics property plays an important role in determining the ultimate photoreactivity.^{32,33} The internal electric fields induced by the unique layered structure would promote the photoinduced charge separation and transfer from the bulk to the surface, which are beneficial to the subsequent photocatalytic reactions on the surface.

With unique layered-structure mediated intriguing properties, bismuth oxyhalide nanomaterials are regarded as promising photocatalysts in the environmental and energy fields. As great advances have been achieved in the research field of bismuth oxyhalide in recent years, two review

articles have emerged recently. Huang et al. gave an overview of engineering the BiOX nanostructures for efficient photocatalytic applications,⁷³ while Ye et al. attempted to review photocatalytic applications of BiOX for environment remediation and their synthesis, modification, facet effects and photocatalytic mechanisms.⁷⁴ Because these two reports mainly focused on the synthesis, properties, and photocatalytic application of bismuth oxyhalide, it remains unclear what are the key factors to govern the growth behaviour of layered structures and how the layered structures affect physicochemical properties and thus photocatalytic mechanisms. More importantly, we still lack a comprehensive review to address some key issues associated with layered structure such as pH related crystal facet exposure and phase transformation mechanisms, facet-dependent molecular oxygen activation pathways, internal electric field tuning, and dehalogenation effect. In view of these concerns, we prepare this feature article.

In this feature article, we first explore the synthesis strategies and growth mechanisms of layered bismuth oxyhalide nanomaterials and then propose design principles of tailoring layered configuration to control nanoarchitectures for favourable photocatalysis. Next, we focus on their layered structure dependent properties including pH related crystal facet exposure and phase transformation, and facet-dependent photoactivity and molecular oxygen activation pathways, so as to clarify the origin of layered structure dependent photoreactivity. In the subsequent section, we summarize various strategies to enhance the photoactivity of nanostructured bismuth oxyhalides. Finally, we highlight some crucial issues in engineering the layered-structure mediated properties of bismuth oxyhalide photocatalysts, and also give tentative suggestions on further increasing their photocatalytic performance.

2. Synthesis of Layered Bismuth Oxyhalides Nanomaterials

One of the intriguing characteristic of bismuth oxyhalide nanomaterials for photocatalytic applications undoubtedly lied in their facile synthesis. As their suitable band-structure for absorbing sunlight to initiate the photocatalytic reaction, the synthesis of well-defined nanostructures ranging from 1-dimension, 2-dimension, 3-dimension, hierarchical, and hollow nanostructure, etc. has become an important task in this research field because their photocatalytic performances highly depend on their structure related characteristics like size, shape, dimensionality, crystal phase, exposed surface and so on.⁷⁵⁻⁷⁷ In this review, we summarize various synthetic strategies for well-defined nanostructures of bismuth oxyhalides as well as their corresponding growth mechanisms as follows.

2.1 Synthesis Strategies of Nanostructured Bismuth Oxyhalides

After the liquid-phase synthesized bismuth oxyhalide was used for the photocatalytic degradation of organic pollutants, the synthesis of bismuth oxyhalide nanostructured photocatalysts has aroused growing interest because they could be easily obtained by simply mixing the bismuth and halogen precursors in the aqueous or organic media at the appropriate ripening temperatures, even room temperature. The most extensively used bismuth sources were $\text{Bi}(\text{NO}_3)_3$, NaBiO_3 and Bi_2O_3 , while $\text{K}(\text{Na})\text{X}$, hexadecyltrimethylammonium chloride (CTAC), hexadecyltrimethylammonium bromide (CTAB), halogen-containing acid and ionic liquid were usually selected as the halogen sources.⁴¹⁻⁵² Besides, BiX_3 ($\text{X} = \text{Cl}, \text{Br}, \text{and I}$) could function as both the bismuth and halogen sources for the synthesis of bismuth oxyhalides. For example, BiOX nanocrystals could be directly obtained by the hydrolysis of BiX_3 .⁶⁷

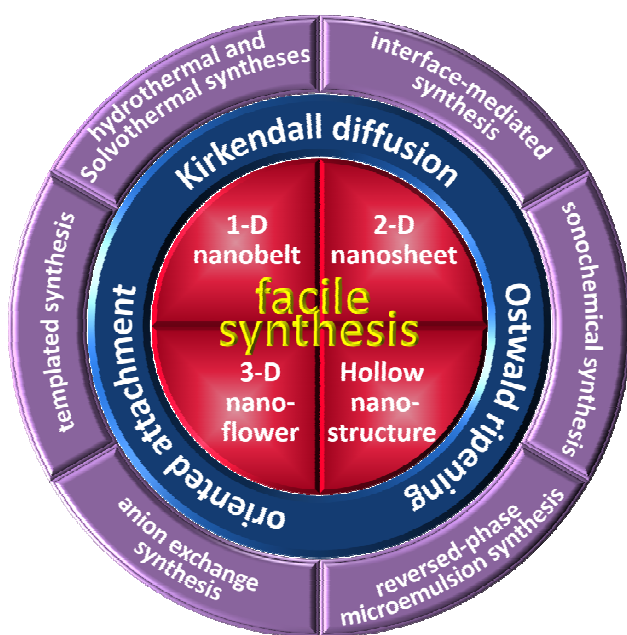


Fig. 1. Schematic illustration of liquid-phase synthesis strategies and growth mechanisms of nanostructured bismuth oxyhalides.

Recent progress has demonstrated that liquid-phase strategies are very powerful for manufacturing desired functional bismuth oxyhalide nanomaterials.^{78,79,81} These liquid-phase synthetic strategies include hydrothermal and solvothermal syntheses, templated synthesis, sonochemical synthesis, interface-mediated synthesis, reversed-phase microemulsion synthesis, and anion exchange synthesis (Fig. 1). Among these synthetic methods, hydrothermal and solvothermal syntheses were the most commonly used approaches to fabricate various nanostructured bismuth oxyhalides. In a hydrothermal or solvothermal system, bismuth oxyhalide nanomaterials were generally synthesized in a sealed vessel with the help of thermal treatment, where the auto-generate pressure upon heating was capable of enhancing the solubility and the reactivity of reactant precursors to initiate the chemical reactions that could not

take place at ambient conditions and also improving the crystallinity.⁸⁰ More importantly, the size, shape, uniformity, dimensionality, crystal phase and exposed crystal facet of as-prepared nanostructured bismuth oxyhalides could be well controlled by tuning the thermodynamic and kinetic parameters of the synthetic system, such as the concentrations of reactant precursors, reaction time, the temperature of thermal treatment, and so on. For example, Zhang et al. hydrothermally synthesized bismuth oxychloride sub-microcrystals with different morphologies from nanoflakes to flower-like and hollow microspheres by facilely adjusting the concentrations of BiCl_3 , poly(vinylpyrrolidone), and citric acid, as well as the relative volume ratio of water to ethanol.⁵³ Also, templated synthesis is another effective strategy for the tunable synthesis of nanostructured bismuth oxyhalides, as this powerful tool usually uses a pre-existing nanostructured template with desired architectural feature as an effective guide to direct the formation of bismuth oxyhalide nanomaterials into various nanostructures that are otherwise difficult to realize.^{82,88} Typically, Wu et al. successfully prepared bismuth oxychloride nanowire arrays with using anodic aluminum oxide (AAO) template-assisted method.²⁸ Meanwhile, other synthetic methods were also applied to prepare various bismuth oxyhalide nanomaterials. For instance, Geng et al. demonstrated the sonochemical synthesis of BiOCl nanosheet in a surfactant/ligand-free system under ambient air.⁴⁵ Xiong et al. employed the interface-mediated route to synthesize hierarchical BiOCl nanospheres via directly reacting metallic Bi nanospheres with FeCl_3 aqueous solution at room temperature.⁴⁸ Henle et al. reported that BiOX nanoparticles of 3-22 nm could be obtained by using reverse microemulsions consisting of heptane, nonionic surfactants, and aqueous salt solutions.⁶⁴ Cheng et al. performed an in situ anion exchange reaction to transform the BiOCl framework into $\text{Bi}_2\text{S}_3/\text{BiOCl}$ hybrid architectures with tunable band gaps by reacting S^{2-} ions released from various sulfur-containing precursors with hierarchical BiOCl architectures.³⁶

2.2 Growth Mechanisms and Design Principles of Layered Configuration Mediated Nanoarchitectures for Bismuth Oxyhalides

It is well established that the formation of nanostructured crystals involves the nucleation, growth and self-assembly processes during the liquid-phase synthesis of semiconductor nanocrystals.^{83,131} Therefore, understanding the initial nucleation mechanism and the following growth process of nanocrystals is a significant prerequisite to arrange the atoms in the solution phase and subsequently realize the controllable synthesis of bismuth oxyhalide nanomaterials with uniform sizes, well-defined morphologies and unique structures. When bismuth and halogen sources are dispersed in the aqueous solution, Bi^{3+} cations are inclined to react with H_2O to yield $(\text{Bi}_2\text{O}_2)^{2+}$ and H^+ cations at the beginning. Then, through coulomb coupling force, the negative X^-

anions will combine with the positive $(\text{Bi}_2\text{O}_2)^{2+}$ cations to form the numerous tiny crystalline nucleus of X-Bi-O-Bi-X, within which the interactions of Bi and O belong to covalent bonds. Meanwhile, the driving force induced by the decrease of total surface energy of crystals will result in the growth and aggregation of X-Bi-O-Bi-X along the direction perpendicular to *c*-axis. This is favorable for the formation of 2-dimension structure of [X-Bi-O-Bi-X] slices. Furthermore, with prolonged ripening time, the fresh tiny [X-Bi-O-Bi-X] slices crystalline nucleus are stacked together by the van der Waals force (nonbonding interaction) through the halogen atoms, thereby yielding various 2-D building blocks. Finally, these individual building blocks will further integrate into various nanostructures via different processes, such as oriented attachment (the assembly of building blocks along specific crystal facet), Kirkendall diffusion (the comparative diffusion rates among different components), and Ostwald ripening (the growth of large precipitates at the expense of smaller precipitates induced by energetic factors), etc.⁸⁴⁻⁸⁷

Besides these well-known self-assembly theories, the assembled behaviors (i.e. growing rate and orientation) of building blocks were also governed by the reaction environment of the solution, such as solvents, impurities, additives, and reaction temperature and time.¹²⁶ Recently, it was reported that ionic liquids were able to induce the formation of various nanostructures of BiOX with ionic liquids functioning as both the solvents and templates to direct the assembly of building blocks. For example, Ma et al. reported that a variety of BiOCl nanostructures, such as ultrathin nanoflakes, nanoplate arrays, and curved nanoplates, could be achieved using an ionic liquid 1-hexadecyl-3-methylimidazolium chloride ($[\text{C}_{16}\text{Mim}]\text{Cl}$) as the “all-in-one” solvent and the structure-directing agent.⁴¹ Furthermore, the additives of organic functional molecules also possess the ability to direct the anisotropic growth of the BiOX nanocrystals and facilitate the generation of various hierarchical architectures. Peng et al. synthesized BiOCl microsphere-, microflower-, and microdisk-like structures assembled with nanoplates via a facile PVP-mediated hydrothermal route.⁶¹ During the synthesis process, PVP not only served as the capping and template-directing agent to promote the oriented growth and assembly of nucleation, but also adsorbed onto the BiOCl surfaces to avoid the random aggregation of individual nanoplates, thus resulting in the construction of various BiOCl hierarchical architectures.

In addition to the aforementioned considerations, the great challenge for the preparation of well-defined structure is the fast nucleation rate of BiOX in the aqueous solution. As the chemical reaction between $(\text{Bi}_2\text{O}_2)^{2+}$ cations and X^- anions is very fast, controlling the formation rate of X-Bi-O-Bi-X nucleation is the key to achieve desired 2-D building blocks, which is beneficial for the tunable synthesis of well-defined morphology and unique hierarchical structure. In general, there are several methods to solve this problem. The first one is to control the hydrolysis rate of bismuth precursors

through adding acids into the bismuth-containing aqueous solution. The acid additives can inhibit the growth of $(\text{Bi}_2\text{O}_2)^{2+}$ cations and favor the reverse reaction to maintain the ionic form of bismuth precursors in aqueous solution. For example, Yu et al. prepared a series of nanostructured BiOX ($\text{X} = \text{Cl}$ and I) ranging from 2-D nanosheet to 3-D hollow microspheres assembled with nanosheets using Bi^{3+} cations as the precursor by dissolving $\text{Bi}(\text{NO}_3)_3$ or BiCl_3 in HNO_3 or HCl aqueous solution.^{53,62,67,155} Another effective method is to yield bismuth-containing coordination compounds by the reaction of bismuth precursors and alcohols. During the nucleation, alcohols could coordinate with Bi^{3+} cations to generate alkoxides complexes. The formation of alkoxides rationally slows the releasing rate of Bi^{3+} cations and thus the growth rate of BiOX crystals. In addition, the greater viscosity of alcoholic solvent could control the supply rate and mobility of building blocks to find the lowest energy configuration interface and subsequently direct their perfectly oriented assemblies to yield various nanostructures. Our group first employed ethylene glycol as the reaction solvent and successfully synthesized 3-D hierarchical BiOX ($\text{X} = \text{Cl}$, Br , I) microspheres assembled with 2-D nanoplates with high photocatalytic activity.⁶⁸ During the growth process, $\text{Bi}(\text{NO}_3)_3$ first coordinated with ethylene glycol to yield alkoxides complexes to control the releasing rate of Bi^{3+} cations, thereby leading to the lower growth rate of X-Bi-O-Bi-X nucleation, which were favorable for the Ostwald-ripening mediated formation of 2-D ultrathin building blocks. Subsequently, the strong viscosity of ethylene glycol and the Kirkendall-diffusion-induced effect upon heating benefited the stack of numerous tiny crystalline nucleus of X-Bi-O-Bi-X to yield a preliminary 3-D configuration, and thus directed the oriented assembly of building blocks to ultimately produce loose microspheres assembled with 2-D nanoplates.

3. Layered Structure Dependent Properties

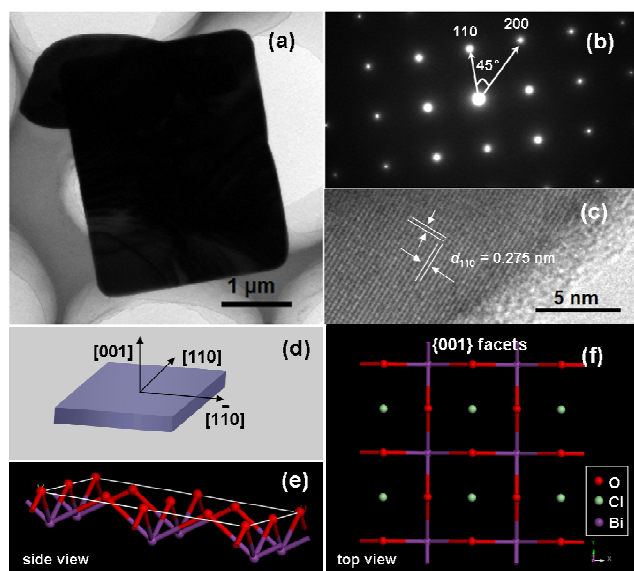
3.1 Layered Structure Dependent Electronic Structures

The layered BiOX ($\text{X} = \text{Cl}$, Br and I) semiconductor materials, as the members of Sillen-Aurivillius family, have a tetragonal PbFCl -type structure (space group P4/nmm) consisting of [X-Bi-O-Bi-X] slices stacked together by the nonbonding (van der Waals) interaction through the halogen atoms along the *c*-axis. In each [X-Bi-O-Bi-X] layer, a bismuth center is surrounded by four oxygen and four halogen atoms, generating an asymmetric decahedral geometry. The interactions within the $[\text{Bi}_2\text{O}_2]$ layers arise from covalent bonds, whereas the [X] layers are stacked together by the van der Waals force (nonbonding interaction) between the X atoms along the *c*-axis. The strong intralayer covalent bonding and the weak interlayer van der Waals interaction can induce the formation of layered structures. For BiOX crystals, the valance band maximum is mainly comprised of O 2p and X np states ($n = 3, 4$ and 5 for $\text{X} =$

Cl, Br and I, respectively) and the Bi 6p states dominate the conduction band minimum.⁸⁹⁻⁹³ As the atomic numbers of X increased, the contribution of X ns states increased remarkably, and the dispersive characteristic of band energy 5 level becomes more and more striking, thereby narrowing the band gap. Obviously, the band gap values and the redox potentials of BiOX are highly associated with the atomic numbers of X, namely the composition of layered structure. Theoretical and experimental studies have shown that the 10 band gaps of BiOCl, BiOBr and BiOI are ca. 3.4, 2.8 and 1.8 eV, respectively. It is evident that the tunable layered structures endowed bismuth oxyhalides materials with excellent optical absorption ranging from UV to visible light, offering their attractive potential for photocatalytic 15 applications.

3.2 Layered Structure Dependent Phase Transformation and Facet Exposure

The layered structure of bismuth oxyhalide is sensitive to the acidity of surrounding environment. In general, the pH value 20 of growth environment had two main effects on the structure and chemical composition, namely pH related crystal facet exposure and phase transformation.



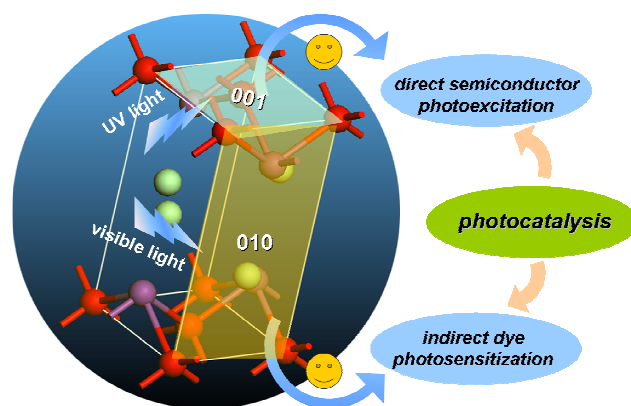
25 **Fig. 2.** (a) TEM image, (b) SAED pattern, and (c) HRTEM image of the BOC-001 SCNSs. (d) Schematic illustration of the crystal orientation of the nanosheet. (e, f) Atomic structure of the {001} facets: (e) side view; (f) top view. Reprinted with permission from ref. 69. Copyright 2012, American Chemical Society.

In the acidic environment, H^+ with a high concentration 30 will modulate the surface adsorption nature of bismuth oxyhalide to further control the facet-selective growth of layered structure to realize the effective engineering of facet exposure. Our group carried out a pioneering work on realizing the different facet exposure of BiOCl.⁶⁹ As the 35 {001} facets of BiOCl have a high density of terminated oxygen atoms and a high surface energy, they will first diminish rapidly during the growth because the evolution of

crystal shape during growth is basically driven by continuously decreasing the total surface energy of crystal.

40 To prevent the disappearance of {001} facets, we intentionally selected H^+ ions as the capping agent to inhibit the growth of (001) plane because of the strong binding interaction between the H^+ ions and terminated oxygen on the (001) surface. As expected, we successfully synthesized 45 {001} facet-dominant BiOCl single-crystalline nanosheets (called as BOC-001) at pH = 1 via a facile hydrothermal route. Meanwhile, {010} facet-dominant BiOCl nanosheets (called as BOC-010) could be fabricated at pH = 6 through adding OH^- ions into the precursor solution because the 50 addition of OH^- ions would decrease the concentration of the H^+ ions and then weaken the binding interaction of H^+ ions and terminated oxygen of (001) surface, which would accelerate the growth of the {010} faceted surface (Fig. 2). Our subsequent theoretical calculation further confirmed the 55 above pH related crystal facet exposure of BiOCl.⁷¹

We interestingly found that the photoactivity of BiOCl nanosheets was highly dependent on the facet exposure. Under UV light, the resulting BiOCl nanosheets with exposed {001} facets exhibited higher direct semiconductor 60 photoexcitation activity for pollutant degradation because of a cooperative effect between the surface atomic structure and suitable internal electric fields. Under visible light, {010} facet-dominant BiOCl nanosheets possessed superior indirect dye photosensitization activity for methyl orange 65 degradation because the larger surface area and open channel characteristic of BiOCl nanosheets with exposed {010} facets could enhance the adsorption capacity of methyl orange molecules and provide more contact sites between the photocatalyst and dye molecules, facilitating more 70 efficient electron injection from the photoexcited dye into the conduction band of the catalyst, favorable for the indirect dye photosensitization process (Fig. 3). These findings not only clarified the origin of facet-dependent photoreactivity of BiOCl nanosheets, but also provided effective guidance 75 for the design and fabrication of highly efficient bismuth oxyhalide photocatalyst.



80 **Fig. 3.** Schematic illustration of facet-dependent photoreactivity of BiOCl single-crystalline nanosheets. Reprinted with permission from ref. 69. Copyright 2012, American Chemical Society.

As soon as the surrounding environment become alkaline, crystal-phase transformation occurred with the substitution of lattice halogen atoms by OH⁻ anions. As mentioned above, bismuth oxyhalides crystallized into unique layered 5 structures consisting of [X-Bi-O-Bi-X] slices stacked together by the nonbonding (van der Waals) interaction between the halogen atoms along the c-axis. In contrast to the strong intralayer covalent bonding of [Bi₂O₂] slabs, the relatively weaker interlayer van der Waals interaction of 10 halogen double slabs makes halogen atoms more active during the chemical reaction. Hence the halogen atoms with weaker van der Waals interaction are more instable than the bismuth and oxygen atoms with covalent bonding. That is, the layered structure of bismuth oxyhalide nanomaterials is 15 very sensitive to the acidity/alkalinity of surrounding environment. Precisely tuning the pH value of growth environment of bismuth oxyhalide nanocrystals could induce the crystal phase transformation into a new layered structure that possessed suitable band structure favorable for the 20 improvement of light absorbance capacity and charge carrier transfer, as well as the position changes of valence and conduction bands. Under the hydrothermal/solvothermal treatment, OH⁻ anions can substitute lattice halogen atoms to break the stoichiometric layered structure and 25 simultaneously form the non-stoichiometric counterpart. The concentration of OH⁻ anions plays a critical role in determining the chemical composition and thus affecting the band structure. With the alkalinity continuously increased, the crystal phase gradually transformed from BiOX (X = Cl, 30 Br, and I) to Bi₁₂O₁₅X₆, Bi₂₄O₃₁X₁₀, Bi₃O₄X, Bi₁₂O₁₇X₂, ultimately Bi₂O₃. For example, our group synthesized Bi₃O₄Cl and Bi₃O₄Br nanosheets via a facile hydrothermal route by controlling the pH values of precursor solutions at 10.3 and 11.5, respectively.^{70,72} When the pH value 35 increased to 12.6, Bi₁₂O₁₇Cl₂ nanobelts were obtained.¹²⁰

3.3 Layered Structure Dependent Oxygen Activation

The first step of the interaction between molecular oxygen and distinct surfaces during photocatalytic process is very important for us to understand the photocatalysis 40 mechanism.⁹⁴⁻⁹⁷ It is well established that molecular oxygen activation plays crucial roles during photocatalysis process because photoinduced electrons on the surface of semiconductors could reduce molecular oxygen to generate reactive oxygen species (ROS) like •O₂⁻, H₂O₂, and •OH, 45 favorable for the pollution degradation, while the effective capture of electrons by molecular oxygen was capable of suppressing the recombination of photoinduced electrons and holes.⁹⁸⁻¹⁰⁹ The molecular oxygen activation pathways highly depended on the first step of sequential reactions on 50 the surface of semiconductors. Therefore, it is tremendously vital to gain in-depth insight into the interaction between molecular oxygen and bismuth oxyhalide semiconductor surfaces, especially how the surface properties of bismuth oxyhalides control the first step of the molecular oxygen 55 activation process.

Another significant reason for exploring the molecular oxygen activation of bismuth oxyhalides lies in our limited knowledge of their molecular oxygen activation mechanism, because most studies focus on the molecular oxygen activation during TiO₂ photocatalysis. It is known that the formation of oxygen vacancies on the materials surface is a prerequisite to the molecular oxygen activation, as the surface oxygen vacancies are the active sites for the molecular oxygen adsorption, while the clean surface usually has a weak affinity to oxygen.^{106,108} Moreover, many reports have demonstrated that molecular oxygen activation pathway relies greatly on the adsorbing capacity of molecular oxygen onto the surface oxygen vacancies of TiO₂ photocatalyst.⁹⁸ Unfortunately, it is difficult to generate 70 oxygen vacancies on the TiO₂ surface, and tune the concentration of surface oxygen vacancies, probably due to the relatively stable surface atomic structure of TiO₂. In contrast, it is much easier to precisely manipulate the molecular oxygen activation pathway for the desired 75 photocatalytic reaction via the creation and modulation of surface oxygen vacancies in bismuth oxyhalides.

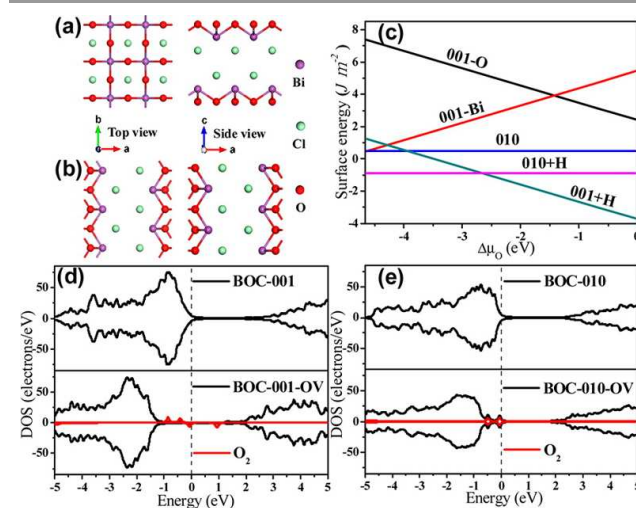


Fig. 4. The structure of (a) (001) and (b) (010) surfaces. (c) The comparison of the calculated surface energy. (d,e) DOS for clean surfaces and surfaces with oxygen vacancies and O₂ adsorption. The positive and negative y values represent majority and minority spin states, respectively. The vertical dashed line shows VBM. Reprinted with permission from ref. 71. Copyright 2013, American Chemical Society.

As one of the most fascinating properties, the unique 85 surface atomic structure of bismuth oxyhalides facilitates the formation of oxygen vacancies under UV light because of the low bond energy and long bond length of the Bi-O bond. This characteristic made them promising alternatives for us to study the relationship between the oxygen vacancies and the molecular oxygen activation pathway.^{94,142} Moreover, the aforementioned {001} and {010} facet-dominant BiOCl nanosheets enable us to compare the molecular oxygen activation pathways on the different facets. We first computationally simulated the molecular oxygen activation 90 processes over {001} and {010} facet-dominant BiOCl nanosheets by calculating the density of states (DOS) and 95 activation process.

charge density difference based on the first-principles calculations.⁷¹ Theoretical calculation results revealed that molecular oxygen could be adsorbed onto the oxygen vacancy sites of {001} facet and form an end-on structure with the two nearest sublayer Bi atoms that extracts one electron from redistributed surface charges to generate $\bullet\text{O}_2^-$. On the {010} facet, O_2 adsorbed on the oxygen vacancy site combines three neighboring Bi atoms to form a complex bridge-on configuration that promotes the simultaneous transfer of two electrons to adsorbed O_2 and generates $\bullet\text{O}_2^{2-}$ species (Fig. 4). Obviously, this result suggested that the molecular oxygen activation pathways of BiOCl nanosheets highly depended on the facet exposure.

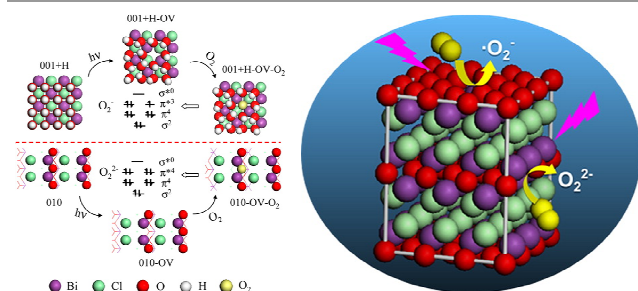


Fig. 5. Proposed molecular oxygen activation processes on BOC-001 and BOC-010 surfaces. Reprinted with permission from ref. 71. Copyright 2013, American Chemical Society.

To confirm these theoretical calculation results, we monitored ROS generation during BOC-001 and BOC-010 photocatalysis under UV light by using electron spin resonance (ESR) techniques to detect the signal of $\bullet\text{O}_2^-$ and photoluminescence method to determine the amount of H_2O_2 , respectively. From ESR spectra we observed a strong four-line ESR signal with the relative intensities of 1:2:2:1 for both BOC-001 and BOC-010. After the same addition of SOD as the scavenger of $\bullet\text{O}_2^-$, the ESR signal intensity of BOC-001 decreased much more remarkably in comparison with that of BOC-010, reflecting that the amount of $\bullet\text{O}_2^-$ generated by BOC-001 was much more than that generated by BOC-010. In addition, more H_2O_2 was generated in the presence of BOC-010. On the basis of theoretical calculations and experimental results, we proposed their molecular oxygen activation mechanisms as follows. Under UV light irradiation, the surfaces of BOC-001 and BOC-010 yielded oxygen vacancies with different structural configuration because of their distinct surface atomic arrangement. Subsequently, the (001) surface of BiOCl preferred to reduce O_2 to $\bullet\text{O}_2^-$ through one-electron transfer, while the (010) surface favored the formation of $\bullet\text{O}_2^{2-}$ via two-electron transfer (Fig. 5). These findings provide atomic-level insight into the photocatalysis mechanism, which deepen our understanding of photocatalytic reaction process for developing high active photocatalysts, and also allow us to selectively manipulate the desired reaction processes via the different molecular oxygen activation pathways. It is believed that the facile synthesis and controllable crystal facet exposure of bismuth oxyhalides as

well as the fast generation of oxygen vacancies under UV light, will stimulate an emerging research interests on the selective manipulation of molecular oxygen activation induced by multiple electron transfer to initiate some specific chemical reactions that can hardly occur at ambient conditions.

4. Layered Structure Tuning for Photoactivity

Enhancement

Bismuth oxyhalide nanomaterials have received immense research interests due to their suitable band structure for absorbing sunlight to initiate the photocatalytic reaction. Unfortunately, their practical applications are still limited by some inherent drawbacks including mismatch between the band gap and light harvesting, inefficient charge separation and transportation, less activity sites, and poor selectivity of desired reaction, etc. For instance, BiOCl is only active in ultraviolet region accounting for about 4% of sunlight. Although BiOBr and BiOI could absorb visible light, the wide band gap of BiOBr still restricts its effective utilization of visible light, while the relatively smaller band-gap of BiOI would inevitably increases the possibility of photogenerated charge carrier recombination. As their photocatalytic properties were highly dependent on the layered structures, various strategies have been developed to engineer the layered structures and overcome these drawbacks. These strategies are summarized as follows.

4.1 Internal Electric Field Tuning

As mentioned above, bismuth oxyhalides possess a unique layered structure characterized by $[\text{Bi}_2\text{O}_2]$ slabs interleaved with halogen slabs. The strong intralayer covalent bonding of $[\text{Bi}_2\text{O}_2]$ slabs and the weak interlayer van der Waals interaction of halogen double slabs would result in the non-uniform charge distribution between $[\text{Bi}_2\text{O}_2]$ and halogen slices, which could polarize the related atoms and orbitals to induce the generation of internal electric field (IEF) along the crystal orientation perpendicular to the $[\text{Bi}_2\text{O}_2]$ and halogen layers. The IEF induced by the unique layered structure could facilitate the separation and transfer of photogenerated charge carrier, thus favorable for the enhancement of photocatalytic performance.

Although the importance of IEF on the photoreactivity enhancement has attracted many attention, almost no progress was made until the emergence of our work on taking advantage of IEF to optimize the photoreactivity of BiOCl.^{20,69,94,95} We found the {001} facet-dominant BiOCl single crystalline nanosheets (BOC SCNSs) exhibited higher direct semiconductor photocatalytic activity toward the degradation of salicylic acid than the {010} facet-dominant nanosheets under ultraviolet irradiation. The higher photoreactivity of {001} facet-dominant BiOCl nanosheets was attributed to the layered-structure mediated IEF, which could induce more efficient photoinduced charge separation and transfer along the [001] direction in the nanosheets than

along the [010] direction to inhibit the recombination of photogenerated electron-hole pairs to increase the photocatalytic degradation of salicylic acid. The high exposure percentage of {001} facet was beneficial for effectively taking advantage of internal electric field to promote the charge transfer and thus increase the photoactivity, which was evidenced by the enhanced photocurrent and quenched photoluminescence signal of {001} facet-dominant nanosheets in comparison with that of {010} facet-dominant counterparts (Fig. 6).

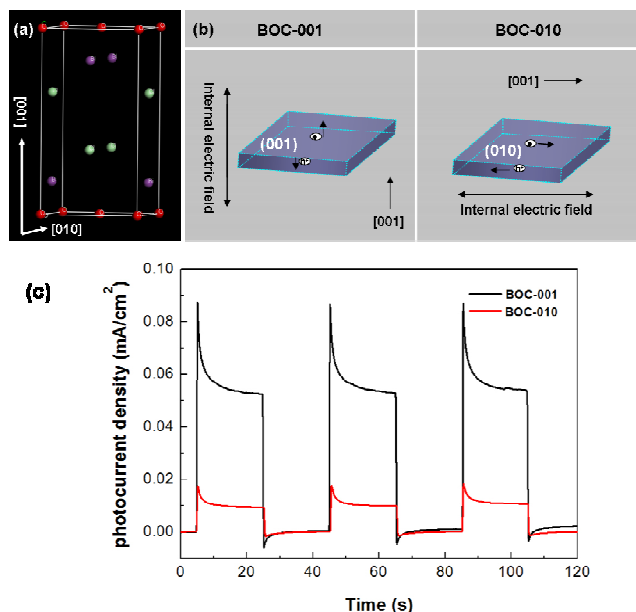


Fig. 6. (a) Crystal structure of BiOCl. (b) Model showing the direction of the internal electric field in each of the BOC SCNs. (c) Photocurrent responses of the BOC SCNs in 0.5 M Na₂SO₄ aqueous solutions under UV-vis irradiation. Reprinted with permission from ref. 69. Copyright 2012, American Chemical Society.

As the photoactivity of layered bismuth oxyhalides is highly correlated with their IEF, it is highly desirable to tune the intensity of IEF. Recently we found that increasing the exposure percentages of {001} facets of Bi₃O₄Cl nanosheets would induce stronger IEF to facilitate the photoreactivity enhancement.⁷² We first prepared a series of Bi₃O₄Cl nanosheets with high {001} facet exposure percentage from 86 to 95% via a facile hydrothermal approach followed with a subsequent liquid phase exfoliation and hydrothermal recrystallization method. The subsequent visible light induced salicylic acid degradation results showed that the photoreactivity of Bi₃O₄Cl nanosheets depended critically on the percentage of exposed {001} facets, while surface properties, crystallinity, light absorbance, and band position were found to have little effect on the photoactivity. Moreover, the charge dynamic property of Bi₃O₄Cl nanosheets had a positive proportional relation with the {001} facet exposure percentage. According to the model developed by Kanata et al. as well as the measured surface voltage and charge density values, we found that the IEF magnitude of Bi₃O₄Cl nanosheets was positively correlated

with the percentage of exposed {001} facets (Fig. 7). A conclusion was then drawn that higher exposure of {001} facets would significantly increase the IEF magnitude and thus further improve the separation and transfer efficiency of photogenerated electron-hole pairs to enhance the photoreactivity. The breakthrough of successfully tuning the intensity of IEF via crystal facet engineering provides new opportunities to greatly improve photocatalytic performance. Tuning the IEF intensity becomes a novel strategy for optimizing the photoreactivity of various layered semiconductor nanomaterials.

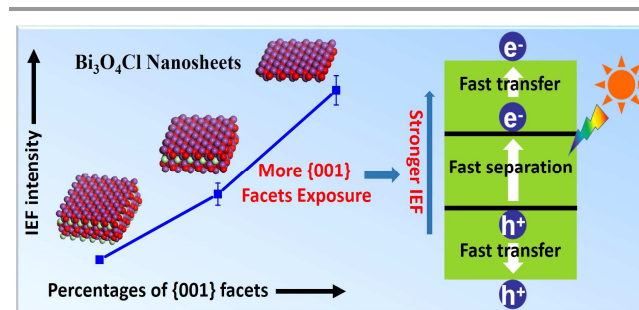


Fig. 7. Proposed mechanism of IEF dependent photocatalytic activity of Bi₃O₄Cl nanosheets. Reprinted with permission from ref. 72. Copyright 2014, Royal Society of Chemistry.

4.2 Dehalogenation Effect

The chemical compositions of semiconductors play pivotal role in determining their band structure, which strongly governs their optical response range, charge carrier mobility, and redox potentials.¹¹⁰⁻¹¹² Therefore, the dehalogenation of bismuth oxyhalides to tune their chemical compositions represents another promising approach for their photocatalytic activity enhancement.

As mentioned previously, bismuth oxyhalides crystallize into unique layered structures consisting of [X-Bi-O-Bi-X] slices stacked together by the nonbonding (van der Waals) interaction between the halogen atoms along the c-axis. These halogen atoms can be easily removed because of their relatively weaker interlayer van der Waals interaction, while the layered structure of bismuth oxyhalide nanomaterials is very sensitive to the surrounding environment, such as the acidity/alkalinity and temperature. The changes of pH value and temperature during the growth of bismuth oxyhalides would result in the dehalogenation, which could induce the transformation of crystal phase to generate chlorine deficient analogue that possessed suitable band structure favorable for the improvement of light absorbance capacity and charge carrier transfer, as well as the position changes of valence and conduction bands.

There are three approaches for the dehalogenation of bismuth oxyhalides, namely alkalization, calcination, and solid-state displacement reaction. The alkalization method is the most extensively employed for the dehalogenation because OH⁻ can replace lattice halogen atoms to break the stoichiometric layered structure and simultaneously form the non-stoichiometric layered structure.^{113-119,207,208} Generally,

the substitution process of lattice halogen atoms occurred when the pH value of precursor solution surroundings exceeded 7. The changes in layered structure and chemical composition of bismuth oxyhalides will alter their corresponding band structure, while their optical absorption edges will vary closely with the molar ratios of O and Bi. Moreover, the modulation of band structure will result in the variation of band redox potential. Recently, we hydrothermally synthesized visible-light-response $\text{Bi}_3\text{O}_4\text{Br}$ nanosheets by adjusting the pH value of the precursor solution to 11.5.¹²⁰ The prepared $\text{Bi}_3\text{O}_4\text{Br}$ photocatalyst exhibited superior catalytic activity to BiOBr . For example, $\text{Bi}_3\text{O}_4\text{Br}$ could completely decompose 40 mg/L sodium pentachlorophenate in 15 min under visible light, while only 10% of removal rate could be achieved in the presence of BiOBr at the same conditions. Density functional theory (DFT) calculation and systematical characterization revealed that high efficient visible-light driven sodium pentachlorophenate removal with $\text{Bi}_3\text{O}_4\text{Br}$ was attributed to effective separation and transfer of photoinduced charge carriers in $\text{Bi}_3\text{O}_4\text{Br}$ with narrower band-gap and more negative conduction band position (Fig. 8), which favored the photogenerated electrons trapping with molecular oxygen to produce $\cdot\text{O}_2^-$. The $\cdot\text{O}_2^-$ radicals could inhibit the recombination of photoinduced charge carriers, and also benefit the dechlorination of chlorinated phenol derivatives.

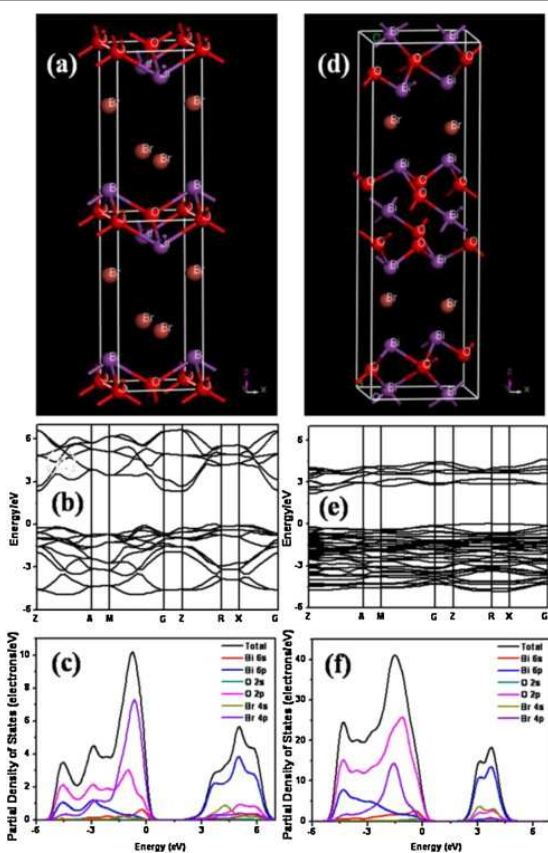


Fig. 8. The crystal structure of BiOBr and $\text{Bi}_3\text{O}_4\text{Br}$ (a, d); calculated band structures of BiOBr and $\text{Bi}_3\text{O}_4\text{Br}$ (b, e); and PDOS of BiOBr and $\text{Bi}_3\text{O}_4\text{Br}$

30 obtained by GGA (c, f). Reprinted with permission from ref. 120. Copyright 2013, Elsevier.

Another approach for the dehalogenation is to directly calcine bismuth oxyhalides in air. Under high temperatures, halogen will be gradually lost, accompanying with different phase transformations. The dehalogenation degree highly depended on the calcination temperature.¹²¹ During the thermal treatment, the O/Bi molar ratios could be controlled continuously by changing the temperature of thermal treatment. For example, Yu et al. obtained BiOBr , $\text{BiOBr}/\text{Bi}_{24}\text{O}_{31}\text{Br}_{10}$, $\text{Bi}_{24}\text{O}_{31}\text{Br}_{10}$, and $\alpha\text{-Bi}_2\text{O}_3$ at various calcination temperatures ranging from 450 to 750 °C.¹²²

Finally, the dehalogenated bismuth oxyhalides could be achieved via the solid-state displacement reaction between BiOX and Bi_2O_3 under high temperature. The content of halogen in bismuth oxyhalides could be tuned by simply altering the molar ratios of BiOX to Bi_2O_3 .^{123,124} For instance, Lin et al. reported the synthesis of $\text{Bi}_3\text{O}_4\text{Cl}$ by calcining the mixed powders of BiOCl and Bi_2O_3 with equal stoichiometric proportion at 700°C in air for 24 h.¹²⁵

50 4.3 Surface Functionalization

Considering the fact that photocatalytic reactions usually took place on the surfaces of semiconductors, the photocatalytic performance is largely dependent on the surface properties of semiconductors.¹²⁶⁻¹³¹ Therefore, surface functionalization of photocatalysts is a promising route to finely tune the photocatalytic performance.

One of the surface functionalization methods is to create oxygen vacancies on the surface of semiconductor.¹³²⁻¹⁴⁰

Oxygen vacancies can offer two main potential benefits for bismuth oxyhalides photocatalysis. First, defects associated with oxygen vacancies can alter the adsorption capacity of gaseous molecules such as CO , H_2O , O_2 , and H_2 on the surface of photocatalysts.¹⁴¹ For instance, in order to investigate the effect of surface structure on the molecular oxygen activation properties, we created oxygen vacancies on the (001) and (010) surfaces of BiOCl to enhance O_2 adsorption via UV light irradiation.⁷¹ The generation of oxygen vacancies under UV light illumination might be attributed to the low bond energy and long bond length of the Bi-O bond. Second, surface oxygen vacancy engineering provides an effective method to modulate the electronic property of bismuth oxyhalide semiconductors, thus increasing the light harvesting and the charge transfer. For example, Ye et al. thought that UV light mediated oxygen vacancy could yield an intermediate state between the valence and conduction bands to narrow the band gap, which made oxygen-deficient BiOCl a promising alternative for visible-light-driven photocatalytic reaction.^{94,142} Our group recently found that reductive ethylene glycol could easily react with oxygen-terminated (001) surface of BiOCl to produce oxygen vacancies at 160 °C, as evidenced by the electron spin resonance (ESR) spectra.¹⁴³ The resulting oxygen vacancies not only extended the light-response edge

up to 650 nm, but also enabled the effective capture of photoinduced electrons and molecular oxygen to generate superoxide anion radicals. Recently, Xie et al. demonstrated that the predominant defects change from isolated defects to triple vacancy associates with the thickness of the {001} facet-dominant BiOCl nanosheets reduced to atomic scale, which could significantly promoted solar-driven photocatalytic activity of BiOCl nanosheets by means of enhancing the adsorption capability and the separation of electron-hole pairs as well as the generation of more reductive photoexcited electrons.²¹

Another surface functionalization is to modify functional organic molecules onto the surface of bismuth oxyhalide nanomaterials as the electron or hole scavengers to suppress the recombination of photoinduced charge carriers.^{144,145} For example, we developed an in situ method to modify ionic liquid [Bmim]I (1-butyl-3-methylimidazolium iodide) onto the BiOI surface by reacting bismuth nitrate with [Bmim]I in water at 70 °C, where the ionic liquid could function as both the iodine source and the surface modified agent. The ionic liquid modification could trap the photoexcited electrons at the conduction band of BiOI to inhibit the recombination of photoinduced electron-hole pairs and thus enhance its photocatalytic activity on the degradation of methyl orange (MO) (Fig. 9).

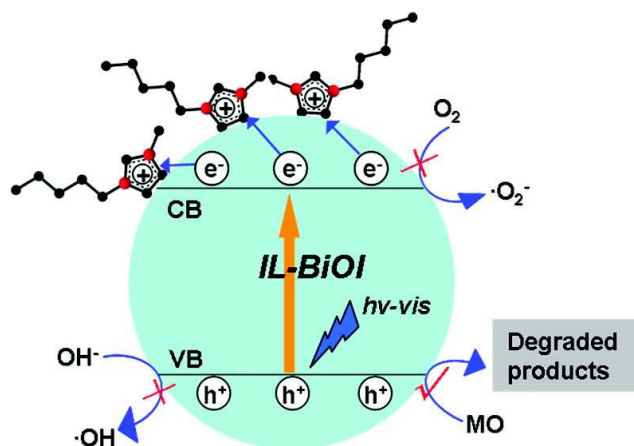


Fig. 9. Schematic illustration of the MO photodegradation process over ionic liquids modified BiOI. Reprinted with permission from ref. 144. Copyright 2011, American Chemical Society.

30 4.4 Doping

Doping is one of the most widely used strategies to increase the photocatalytic activity of semiconductors. Intense research interests have been carried out for semiconductor doping because it is found to be a significant and effective route in modulating the optical and charge dynamics properties as well as the band structures of semiconductors.¹⁴⁶⁻¹⁵³ As BiOCl, BiOBr, and BiOI possess similar layered structure and atomic arrangement as well as chemical composition, which facilitates the incorporation of other halogen atoms into their lattice and subsequently realizes the substitution of each other. Therefore, lots of

halogen-doped bismuth oxyhalide nanomaterials, such as BiOCl_xBr_{1-x}, BiOCl_xI_{1-x} and BiOI_xBr_{1-x}, have been successfully synthesized via a series of wet-chemistry method.¹⁵⁴⁻¹⁶⁵ In contrast, the doping of bismuth oxyhalide semiconductors with foreign element atoms was not as successful as that with halogen doping.^{166,167} This is because that their extremely high symmetry of layered structures would often lead to the poor thermodynamic solubility of heteroatoms in the lattice of bismuth oxyhalides. Moreover, heteroatom doping with introducing foreign element would give rise to the undesirable thermal instability and increased carrier trapping as well as reduced redox reactivity.¹⁶⁸

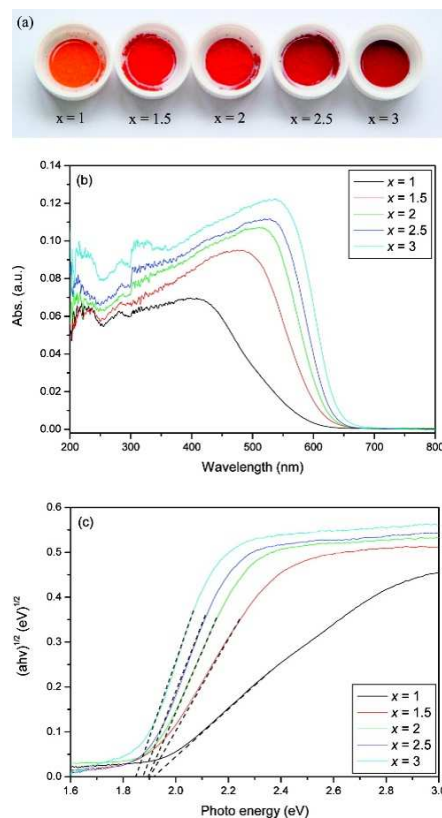


Fig. 10. (a) Gradual color changes of the as-prepared BiOI_x powders. (b) UV-vis diffuse reflectance spectra of BiOI_x powders. (c) Plots of the $(ah\nu)^{1/2}$ vs photon energy (eV) for BiOI_x powders. Reprinted with permission from ref. 68. Copyright 2008, American Chemical Society.

Recently we theoretically and experimentally demonstrated that self doping could tune the surface properties and electronic structures of BiOI without introducing foreign impurity and more defects as the recombination centers for photogenerated carriers.¹⁶⁹ With increasing the molar ratios of I to Bi in the starting reagents, BiOI_x ($x = 1, 1.5, 2, 2.5, \text{ and } 3$) could be easily obtained via a facile soft chemical method. The obvious transition from indirect to direct nature, the depressed conduction band bottom, and the increased composition of s orbital upon iodine self doping provided strong clues that iodine self doping could extend the light response region and also favor the separation of photoinduced electron/hole pairs. The

evident color variation toward the deep red, distinct red-shift of light absorption edge (Fig. 10), and changed valence-band XPS peak configuration of BiOI_x confirmed the formation of new band structure. The enhanced signal intensity in both surface photovoltage spectroscopy and transient photovoltage measurements confirmed the improved charge mobility induced by the new band structure of BiOI_x . Benefited from the effect of iodine self doping, $\text{BiOI}_{1.5}$ exhibited the enhanced photocatalytic activity toward the photodegradation of both methyl orange and NO under visible light than the pristine BiOI. This self-doping approach is highly favorable for the promotion of solar photocatalysis of bismuth oxyhalide nanomaterials.

4.5 The Construction of Plasmonic Photocatalysis System

During the past decade, plasmonic photocatalysis systems composed of metal/semiconductor nanocomposites have gained great attention because they provide a new pathway to engineer the solar energy harvesting processes. In a plasmonic photocatalysis system, plasmonic metal nanoparticles with visible light-harvesting ability were anchored to semiconductor to create a coherent oscillation of the free electrons in resonance with the electrical field of the incoming electromagnetic irradiation, forming so called local surface plasmon resonance (LSPR).¹⁷⁰⁻¹⁷⁴ A wide range of the coupling nanostructures of metal nanoparticles and bismuth oxyhalide semiconductors, including Ag/BiOCl, Ag/BiOBr, Ag/BiOI, Ag-AgX-BiOX (X = Cl, Br, I), have been extensively explored to enhance the photocatalytic activity of bismuth oxyhalides.¹⁷⁵⁻¹⁸³ These plasmonic photocatalysts are generally obtained by loading metallic nanoclusters onto the surface of semiconductor particles via photodeposition and ion exchange reaction methods.

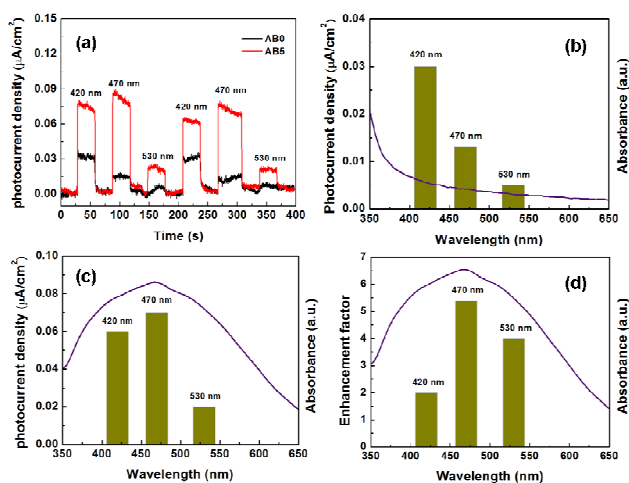


Fig. 11. (a) Photocurrent responses of the AB0 and AB5 in 0.5 M NaSO₄ aqueous solutions under LED light irradiation (420, 470, and 530 nm). (b) Action spectrum of the photocurrent for the AB0 and the UV-vis diffuse reflectance spectrum of AB0 in visible region (solid line). (c) Action spectrum of the photocurrent for the AB5 and UV-vis diffuse reflectance spectrum of AB5 in visible region (solid line). (d) Action spectrum of photocurrent enhancement factor ($I_{\text{AB5}}/I_{\text{AB0}}$) and the UV-vis diffuse reflectance spectrum of AB5 in visible region (solid line). Reprinted with permission from ref. 143. Copyright 2013, Royal Society of Chemistry.

Generally, the shape, size, arrangement, and uniformity of the metal nanoparticles as well as the ratio of metal nanoparticles to semiconductor and so on have significant effects on the surface plasmon resonance (SPR) intensity and wavelength, further affecting the practical performance of plasmonic photocatalysis systems.^{184,185} To gain more favorable photocatalytic performance, it is necessary to well control the nature and alignment of the metal nanoparticles on the semiconductors. For example, we developed an in situ redox-reaction induced deposition approach to synthesize Ag/BiOCl microspheres loaded with Ag nanoparticles of uniform size and shape distribution.¹⁴³ The nonaqueous solvent mediated the generation of oxygen vacancies on the BiOCl surface, ending BiOCl with sufficient reducibility to in situ reduce the metal salt precursors for the subsequent nucleation and growth of metal on the BiOCl surface. During that process, oxygen vacancies guided the growth of Ag nanoparticles, thus resulting in their uniform size and well dispersion. The loading of Ag nanoparticles on BiOCl significantly enhanced the photoreactivity of BiOCl because of SPR effect of nanosized Ag. Meanwhile, irradiation wavelength dependent photocurrent enhancement was found to match well with the UV-vis diffuse reflectance spectrum of the Ag nanoparticles deposited on BiOCl (Fig. 11), which provided direct evidence of plasmonic photocatalysis. These findings provided strong indication that the coupling nanostructures of metal nanoparticles and bismuth oxyhalide semiconductors can increase the optical absorption and favor the separation and transfer of photogenerated charge carrier.

4.6 The Heterojunction Construction

The heterojunction construction is also an effective way to improve the photocatalytic activity of bismuth oxyhalides. The construction of semiconductor heterojunction enables the integration of multiple functional components with the advantages of different components, resulting in higher photocatalytic efficiency than the single semiconductor.¹⁸⁶⁻¹⁹⁰

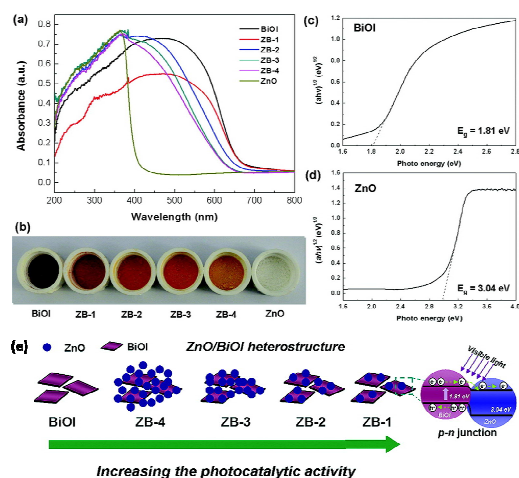


Fig. 12. (a) UV-vis diffuse reflectance spectra and (b) corresponding colors of pure BiOI, pure ZnO, and ZnO/BiOI heterostructures. Plots of $(ah\nu)^{1/2}$ versus

energy (hv) for the band-gap energies of (c) BiOI and (d) ZnO. (e) Schematic illustration of ZnO/BiOI heterostructures with different Bi/Zn molar ratios. Reprinted with permission from ref. 196. Copyright 2011, American Chemical Society.

5 In general, bismuth oxyhalide nanomaterials might play three roles in the semiconductor heterojunction systems. First of all, the band redox potentials of bismuth oxyhalides are in a broad range, so they can easily match with various semiconductors at the energy level to construct an interfacial electric field favorable for the separation and transportation of photogenerated electron-hole pairs. Typical examples of such systems are AgI/BiOI, Bi₂WO₆/BiOI, C₃N₄/BiOBr, and AgBr/BiOBr.¹⁹¹⁻¹⁹⁴ Second, narrow bandgap bismuth oxyhalide semiconductors like BiOI and BiOBr could be employed to photosensitize other wide bandgap semiconductors for the efficient utilization of solar light. For example, we coupled BiOI with TiO₂ and ZnO to construct p-n heterostructures via a facile chemical bath method at low temperature.^{195,196} The morphology, chemical composition, and light response range of TiO₂/BiOI and ZnO/BiOI heterostructures could be controlled by simply adjusting molar ratios of Bi to Ti/Zn in the starting reagents. The more negative conduction band level of BiOI with respect to that of TiO₂ and ZnO would induce the effective transfer of photogenerated electrons from BiOI to TiO₂/ZnO, which extended the light absorption range of TiO₂ and ZnO, and also efficiently inhibited the recombination of electron-hole pairs (Fig. 12). Third, the structural variety of bismuth oxyhalides allowed them to be coupled with carbon-based nanomaterials, especially graphene, to increase the charge separation and transfer.^{197,198} For example, the heterostructures coupling graphene with bismuth oxyhalides, including BiOCl/graphene, BiOBr/graphene, and BiOI/graphene, have been fabricated by utilization of the strong chemical bonding between bismuth oxyhalide and graphene.¹⁹⁹⁻²⁰⁶ In most cases, graphene served as the co-catalyst to extract photogenerated electrons. Therefore, a facile electron transfer from bismuth oxyhalides to graphene can greatly inhibit the electron-hole recombination and thus increase the lifetime of charge carriers, finally enhancing the photocatalytic efficiency.

5. Conclusion Remarks and Perspectives

In recent years bismuth oxyhalide nanomaterials based photocatalysts have attracted worldwide attention, largely inspired by their unique layered-structure mediated intriguing properties and potential applications in the fields of environment remediation and energy conversion. The unique layered structure endowed bismuth oxyhalide nanomaterials with fascinating physicochemical properties like pH related crystal facet exposure and phase transformation, and facet-dependent internal electric field (IEF) intensity. These properties influence their light absorption capacity, photoinduced charge mobility, and band redox potentials. Therefore, the layered structures of bismuth

oxyhalide nanomaterials offer their attractive potential for photocatalytic applications in environment remediation and energy harvesting and open up new pathways for the fundamental study and technological development of layered materials. Although some progresses have been achieved in the field of bismuth oxyhalide photocatalysis, the state-of-the-art bismuth oxyhalide photocatalysts cannot satisfy many requirements of energy and environment applications. In our opinion, some crucial issues in engineering the layered-structure mediated properties of bismuth oxyhalide photocatalysts are still required to be resolved.

First, the powerful theoretical calculations are still on their way to clarify the functions of internal electric field during photocatalysis and to make clear the detailed transfer pathway of photoinduced electrons and holes within the layered structure under the effect of IEF. Besides the crystal facet engineering, more efficient strategies to tune the IEF intensity should be explored, which will boost the development of bismuth oxyhalide nanomaterials.

Second, the correlations between the various nanostructures of bismuth oxyhalides and their photocatalytic activity are still not clear, although intensive efforts have been devoted to the design and synthesis of well-defined nanostructures to optimize the photoreactivity of bismuth oxyhalides. Further systematical investigations are needed to gain in-depth insight into the structure-property relationship of bismuth oxyhalide nanomaterials.

Third, besides the {001} and {010} facet-dominant bismuth oxyhalides, the controlled synthesis of bismuth oxyhalides exposed with other high-energy crystal facets are highly desirable because plenty of atomic steps, dangling bonds, kinks and ledges on reactive high-energy face can act as active sites to facilitate the adsorption of reactant molecules, the surface transfer between photoexcited electrons and reactant molecules, and the desorption of product molecules, thus favoring the photocatalytic reaction. Meanwhile, the successful synthesis of bismuth oxyhalides exposed with different crystal facets allows us to further study their facet dependent properties in more details.

Fourth, the redox nature of different crystal facets of bismuth oxyhalide nanomaterials still remains unclear. As the migration of photoinduced electrons and holes are correlated closely to the facet exposure, there is an urgent demand to clarify the facet-related redox behavior of bismuth oxyhalide nanomaterials, which can provide effective guidance to the design and synthesis of high performance photocatalysts with specific facet exposure for the important oxidative or reductive reactions.

Fifth, the current photocatalytic applications of bismuth oxyhalide nanomaterials mainly focus on the environmental applications. It is necessary to extend their photocatalytic applications to water splitting, CO₂ photoreduction, selective oxidation of organic compounds, etc.

Compared to traditional photocatalysts, such as TiO₂ and ZnO, bismuth oxyhalide photocatalysts are still in their infant stage, which reserves numerous spaces for the further

development. We hope this review on the growth behavior, layered-structure mediated properties and photoactivity enhancement strategies of layered bismuth oxyhalide nanophotocatalysts will have a far-reaching impact on the development of fundamental theory and photocatalytic applications of bismuth oxyhalide nanomaterials in the fields of environmental remediation and energy harvesting.

Acknowledgements

This work was supported by National Basic Research Program of China (973 Program) (Grant 2013CB632402), National Science Foundation of China (Grants 21177048 and 21377044), and Key Project of Natural Science Foundation of Hubei Province (Grant 2013CFA114), and Research Institute of Photocatalysis, State Key Laboratory of Photocatalysis on Energy and Environment.

Notes and references

- ^a Key Laboratory of Pesticide & Chemical Biology of Ministry of Education, Institute of Environmental Chemistry, College of Chemistry, Central China Normal University, Wuhan 430079, P. R. China. E-mail: zhanglz@mail.ccn.edu.cn; Fax/Tel: +86-27-6786 7535
- ^b Institute of Nanoscience and Nanotechnology, College of Physical Science and Technology, Central China Normal University, Wuhan 430079, P. R. China
- 1 A. K. Geim and I. V. Grigorieva, *Nature*, 2013, **499**, 419.
 - 2 M. Chhowalla, H. S. Shin, G. Eda, L. J. Li, K. P. Loh and H. Zhang, *Nat. Chem.*, 2013, **5**, 263.
 - 3 V. Nicolosi, M. Chhowalla, M. G. Kanatzidis, M. S. Strano and J. N. Coleman, *Science*, 2013, **340**, 6139.
 - 4 D. Golberg, Y. Bando, Y. Huang, T. Terao, M. Mitome, C. C. Tang and C. Zhi, *ACS Nano*, 2010, **4**, 2979.
 - 5 M. R. Gao, Y. F. Xu, J. Jiang and S. H. Yu, *Chem. Soc. Rev.*, 2013, **42**, 2986.
 - 6 M. Osada and T. Sasaki, *Adv. Mater.*, 2012, **24**, 210.
 - 7 H. X. Chang and H. K. Wu, *Energy Environ. Sci.*, 2013, **6**, 3483.
 - 8 M. S. Xu, T. Liang, M. M. Shi and H. Z. Chen, *Chem. Rev.*, 2013, **113**, 3766.
 - 9 X. C. Wang, K. Maeda, A. Thomas, K. Takanabe, G. Xin, J. M. Carlsson, K. Domen and M. Antonietti, *Nat. Mater.*, 2009, **8**, 76.
 - 10 Y. Wang, X. C. Wang and M. Antonietti, *Angew. Chem. Int. Ed.*, 2012, **51**, 68.
 - 11 M. M. Lee, J. Teuscher, T. Miyasaka, T. N. Murakami and H. J. Snaith, *Science*, 2012, **338**, 643.
 - 12 S. D. Stranks, G. E. Eperon, G. Grancini, C. Menelaou, M. J. P. Alcocer, T. Leijtens, L. M. Herz, A. Petrozza and H. J. Snaith, *Science*, 2013, **342**, 341.
 - 13 K. Teramura, S. Iguchi, Y. Mizuno, T. Shishido and T. Tanaka, *Angew. Chem. Int. Ed.*, 2012, **51**, 8008.
 - 14 C. G. Silva, Y. Bouzidi, V. Fornés and H. García, *J. Am. Chem. Soc.*, 2009, **131**, 13833.
 - 15 M. A. Loi and J. C. Hummelen, *Nat. Mater.*, 2013, **12**, 1087.
 - 16 S. Dai, Z. Fei, Q. Ma, A. S. Rodin, M. Wagner, A. S. McLeod, M. K. Liu, W. Gannett, W. Regan, K. Watanabe, T. Taniguchi, M. Thiemens, G. Dominguez, A. H. C. Neto, A. Zettl, F. Keilmann, P. Jarillo-Herrero, M. M. Fogler, D. N. Basov, *Science*, 2014, **343**, 1125.
 - 17 J. Rotmensch, J. L. Whitlock, M. L. Dietz, J. J. Hines, R. C. Reba, E. P. Horwitz and P. V. Harper, *Abstr. Pap. Am. Chem. Soc.*, 1998, **216**, U926.
 - 18 G. G. Briand and N. Burford, *Chem. Rev.*, 1999, **99**, 2601.
 - 19 S. K. Poznyak and A. I. Kulak, *Electrochim. Acta*, 1990, **35**, 1941.
 - 20 K. L. Zhang, C. M. Liu, F. Q. Huang, C. Zheng and W. D. Wang, *Appl. Catal., B*, 2006, **68**, 125.
 - 21 M. L. Guan, C. Xiao, J. Zhang, S. J. Fan, R. An, Q. M. Cheng, J. F. Xie, M. Zhou, B. J. Ye and Y. Xie, *J. Am. Chem. Soc.*, 2013, **135**, 10411.
 - 22 Z. H. Ai, W. K. Ho, S. C. Lee and L. Z. Zhang, *Environ. Sci. Technol.*, 2009, **43**, 4143.
 - 23 K. Li, Y. L. Xu, Y. He, C. Yang, Y. L. Wang and J. P. Jia, *Environ. Sci. Technol.*, 2013, **47**, 3490.
 - 24 Y. F. Fang, Y. P. Huang, J. Yang, P. Wang and G. W. Cheng, *Environ. Sci. Technol.*, 2011, **45**, 1593.
 - 25 H. T. Tian, J. W. Li, M. Ge, Y. P. Zhao and L. Liu, *Catal. Sci. Technol.*, 2012, **2**, 2351.
 - 26 F. Chen, H. Q. Liu, S. Bagwasi, X. X. Shen and J. L. Zhang, *J. Photochem. Photobiol. A*, 2010, **215**, 76.
 - 27 J. Xu, W. Meng, Y. Zhang, L. Li and C. S. Guo, *Appl. Catal., B*, 2011, **107**, 355.
 - 28 Z. Y. Yu, B. Detlef, D. Ralf, L. Song and L. Q. Lu, *J. Mol. Catal. A: Chem.*, 2012, **365**, 1.
 - 29 L. Zhang, W. Z. Wang, S. M. Sun, Y. Y. Sun, E. P. Gao and J. Xu, *Appl. Catal., B*, 2013, **132**, 315.
 - 30 R. S. Yuan, S. L. Fan, H. X. Zhou, Z. X. Ding, S. Lin, Z. H. Li, Z. Z. Zhang, C. Xu, L. Wu, X. X. Wang and X. Z. Fu, *Angew. Chem. Int. Ed.*, 2013, **52**, 1035.
 - 31 N. Kijima, K. Matano, M. Saito, T. Oikawa, T. Konishi, H. Yasuda, T. Sato and Y. Yoshimura, *Appl. Catal., A*, 2001, **206**, 237.
 - 32 X. B. Chen and S. S. Mao, *Chem. Rev.*, 2007, **107**, 2891.
 - 33 X. B. Chen, C. Li, M. Gratzel, R. Kostecki and S. S. Mao, *Chem. Soc. Rev.*, 2012, **41**, 7909.
 - 34 Q. F. Zhang, E. Uchaker, S. L. Candelaria and G. Z. Cao, *Chem. Soc. Rev.*, 2013, **42**, 3127.
 - 35 C. F. Guo, S. H. Cao, J. M. Zhang, H. Y. Tang, S. M. Guo, Y. Tian and Q. Liu, *J. Am. Chem. Soc.*, 2011, **133**, 8211.
 - 36 H. F. Cheng, B. B. Huang, X. Y. Qin, X. Y. Zhang and Y. Dai, *Chem. Commun.*, 2012, **48**, 97.
 - 37 Q. H. Mu, Q. H. Zhang, H. Z. Wang and Y. G. Li, *J. Mater. Chem.*, 2012, **22**, 16851.
 - 38 M. Shang, W. Z. Wang and L. Zhang, *J. Hazard. Mater.*, 2009, **167**, 803.
 - 39 Y. Q. Lei, G. H. Wang, S. Y. Song, W. Q. Fan and H. J. Zhang, *CrystEngComm*, 2009, **11**, 1857.
 - 40 J. Y. Xiong, G. Chen, G. F. Li, F. Qin and R. Chen, *RSC Adv.*, 2011, **1**, 1542.
 - 41 J. M. Ma, X. D. Liu, J. B. Lian, X. C. Duan and W. J. Zheng, *Cryst. Growth Des.*, 2010, **10**, 2522.
 - 42 H. Deng, J. W. Wang, Q. Peng, X. Wang and Y. D. Li, *Chem. Eur. J.*, 2005, **11**, 6519.
 - 43 C. Wang, C. Shao, Y. Liu and L. Zhang, *Scr. Mater.*, 2008, **59**, 332.
 - 44 S. J. Wu, C. Wang, Y. F. Cui, T. M. Wang, B. B. Huang, X. Y. Zhang, X. Y. Qin and P. Brault, *Mater. Lett.*, 2010, **64**, 115.
 - 45 J. Geng, W. H. Hou, Y. N. Lv, J. J. Zhu and H. Y. Chen, *Inorg. Chem.*, 2005, **44**, 8503.
 - 46 H. L. Peng, C. K. Chan, S. Meister, X. F. Zhang and Y. Cui, *Chem. Mater.*, 2009, **21**, 247.

- 47 J. Zhang, F. J. Shi, J. Lin, D. F. Chen, J. M. Gao, Z. X. Huang, X. X. Ding and C. C. Tang, *Chem. Mater.*, 2008, **20**, 2937.
- 48 J. Y. Xiong, Z. B. Jiao, G. X. Lu, W. Ren, J. H. Ye and Y. P. Bi, *Chem. Eur. J.*, 2013, **19**, 9472.
- 549 J. M. Song, C. J. Mao, H. L. Niu, Y. H. Shen and S. Y. Zhang, *CrystEngComm*, 2010, **12**, 3875.
- 50 X. Xiao and W. D. Zhang, *J. Mater. Chem.*, 2010, **20**, 5866.
- 51 Y. J. Chen, M. Wen and Q. S. Wu, *CrystEngComm*, 2011, **13**, 3035.
- 1052 L. P. Zhu, G. H. Liao, N. C. Bing, L. L. Wang, Y. Yang and H. Y. Xie, *CrystEngComm*, 2010, **12**, 3791.
- 53 K. Zhang, J. Liang, S. Wang, J. Liu, K. X. Ren, X. Zheng, H. Luo, Y. J. Peng, X. Zou, X. Bo, J. H. Li and X. B. Yu, *Cryst. Growth Des.*, 2012, **12**, 793.
- 1554 H. F. Cheng, B. B. Huang, Z. Y. Wang, X. Y. Qin, X. Y. Zhang and Y. Dai, *Chem. Eur. J.*, 2011, **17**, 8039.
- 55 Y. C. Feng, L. Li, J. W. Li, J. F. Wang and L. Liu, *J. Hazard. Mater.*, 2011, **192**, 538.
- 56 D. Q. Zhang, M. C. Wen, B. Jiang, G. S. Li and J. C. Yu, *J. Hazard. Mater.*, 2012, **211**, 104.
- 2057 R. Hao, X. Xiao, X. X. Zuo, J. M. Nan and W. D. Zhang, *J. Hazard. Mater.*, 2012, **209**, 137.
- 58 Y. N. Huo, J. Zhang, M. Miao and Y. Jin, *Appl. Catal., B*, 2012, **111**, 334.
- 2559 H. F. Cheng, B. B. Huang, Y. Y. Liu, Z. Y. Wang, X. Y. Qin, X. Y. Zhang and Y. Dai, *Chem. Commun.*, 2012, **48**, 9729.
- 60 J. Y. Xiong, G. Chen, F. Qin, R. M. Wang, H. Z. Sun and R. Chen, *Chem. Eng. J.*, 2013, **220**, 228.
- 61 S. J. Peng, L. L. Li, P. N. Zhu, Y. Z. Wu, M. Srinivasan, S. G. Mhaisalkar, S. Ramakrishna and Q. Y. Yan, *Chem. Asian J.*, 2013, **8**, 258.
- 3062 K. X. Ren, K. Zhang, J. Liu, H. D. Luo, Y. B. Huang and X. B. Yu, *CrystEngComm*, 2012, **14**, 4384.
- 63 J. X. Xia, S. Yin, H. M. Li, H. Xu, Y. S. Yan and Q. Zhang, *Langmuir*, 2011, **27**, 1200.
- 3564 J. Henle, P. Simon, A. Frenzel, S. Scholz and S. Kaskel, *Chem. Mater.*, 2007, **19**, 366.
- 65 L. M. Song, S. J. Zhang and Q. W. Wei, *Ind. Eng. Chem. Res.*, 2012, **51**, 1193.
- 4066 J. X. Xia, S. Yin, H. M. Li, H. Xu, L. Xu and Y. G. Xu, *Dalton Trans.*, 2011, **40**, 5249.
- 67 K. Zhang, D. Q. Zhang, J. Liu, K. X. Ren, H. Luo, Y. J. Peng, G. S. Li and X. B. Yu, *CrystEngComm*, 2012, **14**, 700.
- 68 X. Zhang, Z. H. Ai, F. L. Jia and L. Z. Zhang, *J. Phys. Chem. C*, 2008, **112**, 747.
- 4569 J. Jiang, K. Zhao, X. Y. Xiao and L. Z. Zhang, *J. Am. Chem. Soc.*, 2012, **134**, 4473.
- 70 X. Y. Xiao, J. Jiang, and L. Z. Zhang, *Appl. Catal., B*, 2013, **142**, 487.
- 5071 K. Zhao, L. Z. Zhang, J. J. Wang, Q. X. Li, W. W. He and J. J. Yin, *J. Am. Chem. Soc.*, 2013, **135**, 15750.
- 72 J. Li, L. Z. Zhang, Y. J. Li and Y. Yu, *Nanoscale*, 2014, **6**, 167.
- 73 H. F. Cheng, B. B. Huang and Y. Dai, *Nanoscale*, 2014, **6**, 2009.
- 74 L. Q. Ye, Y. R. Su, X. L. Jin, H. Q. Xie and C. Zhang, *Environ. Sci.: Nano*, 2014, **6**, 167.
- 5575 H. Ozawa and K. Sakai, *Chem. Commun.*, 2011, **47**, 2227.
- 76 F. E. Osterloh, *Chem. Soc. Rev.*, 2013, **42**, 2294.
- 77 S. T. Kochuveedu, Y. H. Jang and D. H. Kim, *Chem. Soc. Rev.*, 2013, **42**, 2294.
- 6078 Y. N. Xia, P. D. Yang, Y. G. Sun, Y. Y. Wu, B. Mayers, B. Gates, Y. D. Yin, F. Kim and H. Q. Yan, *Adv. Mater.*, 2003, **15**, 353.
- 79 W. D. Shi, S. Y. Song and H. J. Zhang, *Chem. Soc. Rev.*, 2013, **42**, 5714.
- 80 Z. B. Zhuang, Q. Peng and Y. D. Li, *Chem. Soc. Rev.*, 2011, **40**, 5492.
- 6581 H. C. Zeng, *Acc. Chem. Res.*, 2013, **46**, 226.
- 82 X. W. Lou, L. A. Archer and Z. C. Yang, *Adv. Mater.*, 2008, **20**, 3987.
- 83 D. S. Li, M. H. Nielsen, J. R. I. Lee, C. Frandsen, J. F. Banfield and J. J. D. Yoreo, *Science*, 2012, **336**, 1014.
- 7084 H. C. Zeng, *J. Mater. Chem.*, 2011, **21**, 7511.
- 85 Y. D. Yin, R. M. Rioux, C. K. Erdonmez, S. Hughes, G. A. Somorjai and A. P. Alivisatos, *Science*, 2004, **304**, 711.
- 86 H. J. Fan, M. Knez, R. Scholz, K. Nielsch, E. Pippel, D. Hesse, M. Zacharias and U. Gösele, *Nat. Mater.*, 2006, **5**, 627.
- 7587 B. Liu and H. C. Zeng, *Small*, 2005, **1**, 566.
- 88 Y. D. Liu, J. Goebel and Y. D. Yin, *Chem. Soc. Rev.*, 2013, **42**, 2610.
- 89 L. J. Zhao, X. C. Zhang, C. M. Fan, Z. H. Liang and P. D. Han, *Physica. B*, 2012, **407**, 3364.
- 8090 X. C. Zhang, L. J. Zhao, C. M. Fan, Z. H. Liang and P. D. Han, *Comput. Mater. Sci.*, 2012, **61**, 180.
- 91 H. J. Zhang, L. Liu and Z. Zhou, *RSC Adv.*, 2012, **2**, 9224.
- 92 W. C. Wang, W. J. Yang, R. Chen, X. B. Duan, Y. L. Tian, D. W. Zeng and B. Shan, *Phys. Chem. Chem. Phys.*, 2012, **14**, 2450.
- 8593 H. J. Zhang, L. Liu and Z. Zhou, *Phys. Chem. Chem. Phys.*, 2012, **14**, 1286.
- 94 L. Q. Ye, L. Zan, L. H. Tian, T. Y. Peng and J. J. Zhang, *Chem. Commun.*, 2011, **47**, 6951.
- 9095 L. Q. Ye, L. H. Tian, T. Y. Peng and L. Zan, *J. Mater. Chem.*, 2011, **21**, 12479.
- 96 D. Zhang, J. Li, Q. G. Wang and Q. S. Wu, *J. Mater. Chem. A*, 2013, **1**, 8622.
- 97 D. H. Wang, G. Q. Gao, Y. W. Zhang, L. S. Zhou, A. W. Xu and W. Chen, *Nanoscale*, 2012, **4**, 7780.
- 9598 A. L. Linsebigler, G. Q. Lu and J. T. Yates, Jr, *Chem. Rev.*, 1995, **95**, 735.
- 99 L. Khachatryan, E. Vejerano, S. Lomnicki and B. Dellinger, *Environ. Sci. Technol.*, 2011, **45**, 8559.
- 100100 S. J. Tan, Y. F. Ji, Y. Zhao, A. D. Zhao, B. Wang, J. L. Yang and J. G. Hou, *J. Am. Chem. Soc.*, 2011, **133**, 2002.
- 101 M. A. Henderson and I. Lyubinetsky, *Chem. Rev.*, 2013, **113**, 4428.
- 102 C. C. Chen, W. H. Ma and J. C. Zhao, *Chem. Soc. Rev.*, 2010, **39**, 4206.
- 105103 Y. B. Zhao, W. H. Ma, Y. Li, H. W. Ji, C. C. Chen, H. Y. Zhu and J. C. Zhao, *Angew. Chem. Int. Ed.*, 2012, **51**, 3188.
- 104 H. Sheng, H. W. Ji, W. H. Ma, C. C. Chen and J. C. Zhao, *Angew. Chem. Int. Ed.*, 2013, **52**, 9686.
- 105 Y. Li, W. Zhang, J. F. Niu and Y. S. Chen, *ACS Nano*, 2012, **6**, 5164.

- 106 E. Wahlström, E. K. Vestergaard, R. Schaub, A. Rønna, M. Vestergaard, E. Lægsgaard, I. Stensgaard and F. Besenbacher, *Science*, 2004, **303**, 511.
- 107 Y. B. He, A. Tilocca, O. Dulub, A. Selloni and U. Diebold, *Nat. Mater.*, 2009, **8**, 585.
- 108 R. Schaub, E. Wahlström, A. Rønna, E. Lægsgaard, I. Stensgaard and F. Besenbacher, *Science*, 2003, **299**, 377.
- 109 M. Lazzeri, A. Vittadini and A. Selloni, *Phys. Rev. B*, 2001, **63**, 155409.
- 110 A. M. Smith and S. M. Nie, *Acc. Chem. Res.*, 2010, **43**, 190.
- 111 D. Q. Zhang, G. S. Li, H. X. Li and Y. F. Lu, *Chem. Asian J.*, 2013, **8**, 26.
- 112 L. W. Zhang and Y. F. Zhu, *Catal. Sci. Technol.*, 2012, **2**, 694.
- 113 X. Xiao, C. Liu, R. P. Hu, X. X. Zuo, J. M. Nan, L. S. Li and L. S. Wang, *J. Mater. Chem.*, 2012, **22**, 22840.
- 114 Y. Y. Li, H. C. Yao, J. S. Wang, N. Wang and Z. J. Li, *Mater. Res. Bull.*, 2011, **46**, 292.
- 115 S. M. Sun, W. Z. Wang, L. Zhang, L. Zhou, W. Z. Yin and M. Shang, *Environ. Sci. Technol.*, 2009, **43**, 2005.
- 116 J. Cao, X. Li, H. L. Lin, B. Y. Xu, B. D. Luo and S. F. Chen, *Mater. Lett.*, 2012, **76**, 181.
- 117 X. Xiao, R. Hao, X. X. Zuo, J. M. Nan, L. S. Li and W. D. Zhang, *Chem. Eng. J.*, 2012, **209**, 293.
- 118 X. Xiao and W. D. Zhang, *RSC Adv.*, 2011, **1**, 1099.
- 119 G. Chen, G. L. Fang and G. D. Tang, *Mater. Res. Bull.*, 2013, **48**, 1256.
- 120 J. L. Wang, Y. Ying and L. Z. Zhang, *Appl. Catal., B*, 2013, **136**, 112.
- 121 L. Armelao, G. Bottaro, C. Y. Maccato and E. Tondello, *Dalton Trans.*, 2012, **41**, 5480.
- 122 C. L. Yu, W. Q. Zhou, J. C. Yu, F. F. Cao and X. Li, *Chin. J. Chem.*, 2012, **30**, 721.
- 123 B. F. Gao, A. K. Chakraborty, J. M. Yang and W. I. Lee, *Bull. Korean Chem. Soc.*, 2010, **31**, 1941.
- 124 A. K. Chakraborty and M. A. Kebede, *Reac. Kinet. Mech. Cat.*, 2012, **106**, 83.
- 125 X. P. Lin, T. Huang, F. Q. Huang, W. D. Wang and J. L. Shi, *J. Phys. Chem. B*, 2006, **110**, 24629.
- 126 L. Q. Jing, W. Zhou, G. H. Tian and H. G. Fu, *Chem. Soc. Rev.*, 2013, **42**, 9509.
- 127 Z. Y. Zhou, N. Tian, J. T. Li, I. Broadwell and S. G. Sun, *Chem. Soc. Rev.*, 2011, **40**, 4167.
- 128 C. T. Campbell and J. Sauer, *Chem. Rev.*, 2013, **113**, 3859.
- 129 F. Caruso, *Adv. Mater.*, 2001, **13**, 11.
- 130 M. Batzill, *Energy Environ. Sci.*, 2011, **4**, 3275.
- 131 G. Liu, J. C. Yu, G. Q. Lu and H. M. Cheng, *Chem. Commun.*, 2011, **47**, 6763.
- 132 X. W. Liu, K. B. Zhou, L. Wang, B. Y. Wang and Y. D. Li, *J. Am. Chem. Soc.*, 2009, **131**, 3140.
- 133 G. Liu, H. G. Yang, X. W. Wang, L. N. Cheng, H. F. Lu, L. Z. Wang, H. M. Cheng and G. Q. Lu, *J. Phys. Chem. C*, 2009, **113**, 21784.
- 134 Q. P. Wu and R. V. Krol, *J. Am. Chem. Soc.*, 2012, **134**, 9369.
- 135 Z. F. Zheng, J. Teo, X. Chen, H. W. Liu, Y. Yuan, E. R. Waclawik, Z. Y. Zhong and H. Y. Zhu, *Chem. Eur. J.*, 2010, **16**, 1202.
- 136 T. R. Gordon, M. Cargnello, T. Paik, F. Mangolini, R. T. Weber, P. Fornasiero and C. B. Murray, *J. Am. Chem. Soc.*, 2012, **134**, 6751.
- 137 R. Schaub, P. Thosttrup, N. Lopez, E. Lægsgaard, I. Stensgaard, J. K. Nørskov and F. Besenbacher, *Phys. Rev. Lett.*, 2001, **87**, 266104.
- 138 M. Setvin, U. Aschauer, P. Scheiber, Y. F. Li, W. Y. Hou, M. Schmid, A. Selloni and U. Diebold, *Science*, 2013, **341**, 988.
- 139 W. Gopel, G. Rocker and R. Feierabend, *Phys. Rev. B*, 1983, **28**, 3427.
- 140 A. Linsebigler, G. Lu and J. J. T. Yates, *J. Chem. Phys.*, 1995, **103**, 9438.
- 141 X. Y. Pan, M. Q. Yang, X. Z. Fu, N. Zhang and Y. J. Xu, *Nanoscale*, 2013, **5**, 3601.
- 142 L. Q. Ye, K. J. Deng, F. Xu, L. H. Tian, T. Y. Peng and L. Zan, *Phys. Chem. Chem. Phys.*, 2012, **14**, 82.
- 143 J. Jiang, L. Z. Zhang, H. Li, W. W. He and J. J. Yin, *Nanoscale*, 2013, **5**, 10573.
- 144 Y. N. Wang, K. J. Deng and L. Z. Zhang, *J. Phys. Chem. C*, 2011, **115**, 14300.
- 145 G. H. Dong and L. Z. Zhang, *J. Phys. Chem. C*, 2013, **117**, 4062.
- 146 D. J. Norris, A. L. Efros and S. C. Erwin, *Science*, 2008, **319**, 1776.
- 147 G. Liu, L. Z. Wang, H. G. Yang, H. M. Cheng and G. Q. Lu, *J. Mater. Chem.*, 2010, **20**, 831.
- 148 R. Asahi, T. Morikawa, T. Ohwaki, K. Aoki and Y. Taga, *Science*, 2001, **293**, 269.
- 149 S. U. M. Khan, M. Al-Shahry and W. B. Ingler, *Science*, 2002, **297**, 2243.
- 150 J. C. Yu, J. G. Yu, W. Ho, Z. T. Jiang and L. Z. Zhang, *Chem. Mater.*, 2002, **14**, 3808.
- 151 W. Zhao, W. H. Ma, C. C. Chen, J. C. Zhao and Z. G. Shuai, *J. Am. Chem. Soc.*, 2004, **126**, 4782.
- 152 G. Liu, Y. N. Zhao, C. H. Sun, F. Li, G. Q. Lu and H. M. Cheng, *Angew. Chem. Int. Ed.*, 2008, **47**, 4516.
- 153 J. Wang, D. N. Tafen, J. P. Lewis, Z. L. Hong, A. Manivannan, M. J. Zhi, M. Li and N. Q. Wu, *J. Am. Chem. Soc.*, 2009, **131**, 12290.
- 154 H. G. Gnayem and Y. Sasson, *ACS Catal.*, 2013, **3**, 186.
- 155 K. X. Ren, J. Liang, J. Liu, K. Zhang, X. Zheng, H. D. Luo, Y. B. Huang, P. J. Liu and X. B. Yu, *Dalton Trans.*, 2013, **42**, 9706.
- 156 T. B. Li, G. Chen, C. Zhou, Z. Y. Shen, R. C. Jin and J. X. Sun, *Dalton Trans.*, 2011, **40**, 6751.
- 157 Y. Y. Liu, W. J. Son, J. B. Lu, B. B. Huang, Y. Dai and M. H. Whangbo, *Chem. Eur. J.*, 2011, **17**, 9342.
- 158 Z. F. Jia, F. M. Wang, F. Xin and B. Q. Zhang, *Ind. Eng. Chem. Res.*, 2011, **50**, 6688.
- 159 J. Cao, B. Y. Xu, B. D. Luo, H. L. Lin and S. F. Chen, *Catal. Commun.*, 2011, **13**, 63.
- 160 F. Dong, Y. J. Sun, M. Fu, Z. B. Wu and S. C. Lee, *J. Hazard. Mater.*, 2012, **219**, 26.
- 161 X. Xiao, R. Hao, M. Liang, X. X. Zuo, J. M. Nan, L. S. Li and W. D. Zhang, *J. Hazard. Mater.*, 2012, **233**, 122.
- 162 S. Shenawi-Khalil, V. Uvarov, S. Fronton, I. Popov and Y. Sasson, *Appl. Catal., B*, 2012, **117**, 148.

- 163 W. J. Kim, D. Pradhan, B. Min and Y. Sohn, *Appl. Catal., B*, 2014, **147**, 711.
- 164 B. Zhang, G. B. Ji, Y. S. Liu, M. A. Gondal and X. F. Chang, *Catal. Commun.*, 2013, **36**, 25.
- 5 165 S. Shenawi-Khalil, V. Uvarov, Y. Kritsman, E. Menes, I. Popov and Y. Sasson, *Catal. Commun.*, 2011, **12**, 1136.
- 166 B. Pare, B. Sarwan and S. B. Jonnalagadda, *Appl. Surf. Sci.*, 2011, **258**, 247.
- 167 J. H. Yu, B. Wei, L. Zhu, H. Gao, W. J. Sun and L. L. Xu, *Appl. Surf. Sci.*, 2013, **284**, 497.
- 10 168 G. H. Dong, K. Zhao and L. Z. Zhang, *Chem. Commun.*, 2012, **48**, 6178.
- 169 X. Zhang and L. Z. Zhang, *J. Phys. Chem. C*, 2010, **114**, 18198.
- 170 S. Linic, P. Christopher and D. B. Ingram, *Nat. Mater.*, 2011, **10**, 911.
- 15 171 W. B. Hou and S. B. Cronin, *Adv. Funct. Mater.*, 2013, **23**, 1612.
- 172 P. Wang, B. B. Huang, Y. Dai and M. H. Whangbo, *Phys. Chem. Chem. Phys.*, 2012, **14**, 9813.
- 173 S. C. Warren and E. Thimsen, *Energy Environ. Sci.*, 2012, **5**, 5133.
- 20 174 I. Thomann, B. A. Pinaud, Z. B. Chen, B. M. Clemens, T. F. Jaramillo and M. L. Brongersma, *Nano Lett.*, 2011, **11**, 3440.
- 175 H. Liu, W. R. Cao, Y. Su, Y. Wang and X. H. Wang, *Appl. Catal., B*, 2012, **111**, 271.
- 25 176 C. L. Yu, C. F. Fan, X. J. Meng, K. Yang, F. F. Cao and X. Li, *Reac. Kinet. Mech. Cat.*, 2011, **103**, 141.
- 177 H. F. Cheng, B. B. Huang, P. Wang, Z. Y. Wang, Z. Z. Lou, J. P. Wang, X. Y. Qin, X. Y. Zhang and Y. Dai, *Chem. Commun.*, 2011, **47**, 7054.
- 30 178 W. Xiong, Q. D. Zhao, X. Y. Li and D. K. Zhang, *Catal. Commun.*, 2011, **16**, 229.
- 179 L. Q. Ye, J. Y. Liu, C. Q. Gong, L. H. Tian, T. Y. Peng and L. Zan, *ACS Catal.*, 2012, **2**, 1677.
- 180 J. Cao, Y. J. Zhao, H. L. Lin, B. Y. Xu and S. F. Chen, *J. Solid. State. Chem.*, 2013, **206**, 38.
- 35 181 Y. Q. Lei, G. H. Wang, P. R. Guo and H. C. Song, *Appl. Surf. Sci.*, 2013, **279**, 374.
- 182 L. F. Lu, L. Kong, Z. Jiang, H. Lai, T. C. Xiao and P. P. Edwards, *Catal. Lett.*, 2012, **142**, 771.
- 40 183 J. Di, J. X. Xia, S. Yin, H. Xu, M. Q. He, H. M. Li, L. Xu and Y. P. Jiang, *RSC Adv.*, 2013, **3**, 19624.
- 184 H. Tong, S. X. Ouyang, Y. P. Bi, N. Umezawa, M. Oshikiri and J. H. Ye, *Adv. Mater.*, 2012, **24**, 229.
- 185 S. Linic, P. Christopher, H. L. Xin and A. Marimuthu, *Acc. Chem. Res.*, 2013, **46**, 1890.
- 45 186 Y. Q. Qu and X. F. Duan, *Chem. Soc. Rev.*, 2013, **42**, 2568.
- 187 X. J. Lang, X. D. Chen and J. C. Zhao, *Chem. Soc. Rev.*, 2014, **43**, 473.
- 188 F. Y. Wen and C. Li, *Acc. Chem. Res.*, 2013, **46**, 2355.
- 50 189 P. D. Tran, L. H. Wong, J. Barber and J. S. C. Loo, *Energy Environ. Sci.*, 2012, **5**, 5902.
- 190 J. H. Yang, D. E. Wang, H. X. Han and C. Li, *Acc. Chem. Res.*, 2013, **46**, 1900.
- 191 H. F. Cheng, B. B. Huang, Y. Dai, X. Y. Qin and X. Y. Zhang, *Langmuir*, 2010, **26**, 6618.
- 55 192 H. Q. Li, Y. M. Cui and W. S. Hong, *Appl. Surf. Sci.*, 2013, **264**, 581.
- 193 L. Kong, Z. Jiang, H. H. Lai, R. J. Nicholls, T. C. Xiao, M. O. Jones and P. P. Edwards, *J. Catal.*, 2012, **293**, 116.
- 60 194 J. Fu, Y. L. Tian, B. B. Chang, F. N. Xi and X. P. Dong, *J. Mater. Chem.*, 2012, **22**, 21159.
- 195 X. Zhang, L. Z. Zhang, T. F. Xie and D. J. Wang, *J. Phys. Chem. C*, 2009, **113**, 7371.
- 196 J. Jiang, X. Zhang, P. B. Sun and L. Z. Zhang, *J. Phys. Chem. C*, 2011, **115**, 20555.
- 65 197 Q. J. Xiang, J. G. Yu and M. Jaroniec, *Chem. Soc. Rev.*, 2012, **41**, 782.
- 198 W. G. Tu, Y. Zhou and Z. G. Zou, *Adv. Funct. Mater.*, 2013, **23**, 4996.
- 70 199 F. D. Gao, D. W. Zeng, Q. W. Huang, S. Q. Tian and C. S. Xie, *Phys. Chem. Chem. Phys.*, 2012, **14**, 10572.
- 200 S. Y. Song, W. Gao, X. Wang, X. Y. Li, D. P. Liu, Y. Xing and H. J. Zhang, *Dalton Trans.*, 2012, **41**, 10472.
- 201 X. M. Tu, S. L. Luo, G. X. Chen and J. H. Li, *Chem. Eur. J.*, 2012, **18**, 14359.
- 75 202 H. Liu, Y. Su, Z. Chen, Z. T. Jin and Y. Wang, *J. Hazard. Mater.*, 2014, **266**, 75.
- 203 H. Liu, W. R. Cao, Y. Su, Z. Chen and Y. Wang, *J. Colloid. Interface. Sci.*, 2013, **398**, 161.
- 80 204 Z. Liu, W. C. Xu, J. Z. Fang, X. X. Xu, S. X. Wu, X. M. Zhu and Z. H. Chen, *Appl. Surf. Sci.*, 2012, **259**, 441.
- 205 Z. H. Ai, W. Ho and S. C. Lee, *J. Phys. Chem. C*, 2011, **115**, 25330.
- 206 X. M. Zhang, X. F. Chang, M. A. Gondal, B. Zhang, Y. S. Liu and G. B. Ji, *Appl. Surf. Sci.*, 2012, **258**, 7826.
- 85 207 J. Shang, W. C. Hao, X. J. Lv, T. M. Wang, X. L. Wang, Y. Du, S. X. Dou, T. F. Xie, D. J. Wang and J. Wang, *ACS Catal.*, 2014, **4**, 954.
- 208 H. L. Chen, W. W. Lee, W. H. Chung, H. P. Lin, Y. J. Chen, Y. R. Jiang, W. Y. Lin and C. C. Chen, *J. Taiwan. Inst. Chem. Eng.*, 2014, <http://dx.doi.org/10.1016/j.jtice.2013.12.015>.
- 90